Science of the Total Environment 703 (2020) 134718

Contents lists available at ScienceDirect

Science of the Total Environment

journal homepage: www.elsevier.com/locate/scitotenv

Desiccation crisis of saline lakes: A new decision-support framework for building resilience to climate change

Amirhossein Hassani [a], Adisa Azapagic [a,*], Paolo D'Odorico [b], Amir Keshmiri [c], Nima Shokri [a,*]

[a] Department of Chemical Engineering and Analytical Science, The University of Manchester, Manchester, UK
[b] Department of Environmental Science, Policy & Management, UC Berkeley, CA, USA
[c] Department of Mechanical, Aerospace & Civil Engineering, The University of Manchester, Manchester, UK

HIGHLIGHTS

- An eco-hydrological framework is developed to restore desiccating saline lakes.
- A wide range of climatic, hydrologic, and agronomic stressors are considered.
- Parts of the lake that should be prioritized for restoration can also be identified.
- Alternative cropping patterns and land-use change are determined for restoration.
- The framework applicability is demonstrated through the case of Lake Urmia in Iran.

GRAPHICAL ABSTRACT

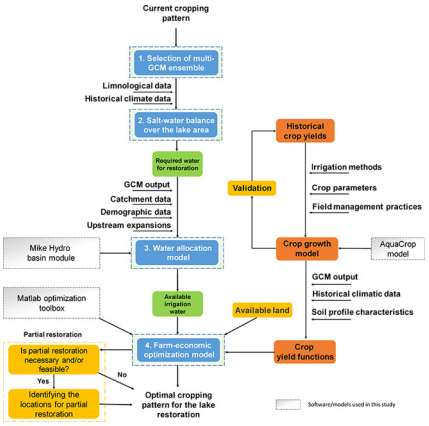

ARTICLE INFO

Article history:
Received 3 July 2019
Received in revised form 27 September 2019
Accepted 27 September 2019
Available online 19 October 2019

Editor: Damia Barcelo

Keywords:
Ecosystem services
Lake restoration
Lake Urmia
Land use management
Optimal cropping patterns
Saline lakes

ABSTRACT

River flow reductions as a result of agricultural withdrawals and climate change are rapidly desiccating endorheic lakes, increasing their salinity and affecting the bio-diversity and human wellbeing in the surrounding areas. Here we present a new framework to guide eco-hydrological restoration of saline lakes and build their resilience to climate change by optimizing agricultural land use and related water withdrawals. The framework involves four steps: 1. selection of global circulation models for the basin under study; 2. establishment of a hydrological balance over the lake's area to estimate the amount of water required for its restoration; 3. water allocation modeling to determine the water available for restoration and allocation of the remaining water across different users in the lake's basin; and 4. basin-scale optimization of land use and cropping patterns subject to water availability. We illustrated the general applicability of the framework through the case of the second largest (by volume) hyper-saline lake globally, Lake Urmia, which lost 96% of its volume in only 20 years, primarily as a result of upstream water withdrawals. Through the application of the framework, we estimated the amount of water needed to restore the lake, either fully or partially, and proposed a sustainable land-use strategy, while protect farmers' income in the basin. Considering future climate change projections under two representative concentration pathways (RCP) 4.5 and 8.5, we found that an average annual surface inflow of 3,648 Mm^3 (~70% increase in RCP 4.5) and 3,692 Mm^3 (~73% increase in RCP 8.5) would be required to restore the lake by 2050, respectively. This would require the respective conversion of 95,600 ha and 133,687 ha of irrigated land to rain-fed cropland or grassland across the basin by 2050. The proposed framework can be

* Corresponding authors.
E-mail addresses: adisa.azapagic@machester.ac.uk (A. Azapagic), nima.shokri@manchester.ac.uk (N. Shokri).

https://doi.org/10.1016/j.scitotenv.2019.134718

Nomenclature

a, b	Constants in subsidy function
A	Total area under cultivation (ha)
a_c, b_c, c_c	Calibration parameters in the lake level-volume relation
AOT	Aerosol optical thickness
C_α, C_β	Constant parameters in Eq. (10)
C_a	Production cost (US$ ha^{-1})
CC_x	Maximum canopy cover
c_y	Dimensionless coefficient used in Eq. (11)
d_1	Lower saltating particle size (m)
d_2	Upper saltating particle size (m)
Δd_i	Particle-size bin interval length (m)
d_i	Particle-size bin mean diameter (m)
D_j	Mean diameter of jth mode (m)
d_s	Particle size (m)
e_f	Freshwater pan evaporation (mm yr^{-1})
e_s	Lake water pan evaporation (mm yr^{-1})
η_f	The total fraction of dust which can be released from unit soil mass
f	Dust fraction in soil
F	Vertical dust flux (kg m^{-2} s^{-1})
$F(Y)$	Crop-field production function (t ha^{-1})
g	Acceleration due to gravity (m s^{-2})
i	Number of cultivated crops
I	Number of particle-size bins
J	Number of modes in calculation of fully/minimally particle size distribution
Δm	Change in the mass of lake brine after Δt (kg)
$m_{evaporation}$	Mass of evaporated water from the lake area (kg)
$m_{\inf}$	Mass of water entered to the lake by rivers (kg)
m_{pre}	Mass of precipitation over the lake area (kg)
$m_{saltavailable}$	Available salt mass in the lake (kg)
m_{salt}	Change in the mass of lake water salt after Δt (kg)
$m_{saltnew}$	Salt mass available in the lake after Δt (kg)
$m_{saltrivers}$	Salt mass added by rivers (kg)
ω	Function used in Eq. (7)
p	Soil surface plastic pressure (Pa)
P_c	Income received by farmers (US$ t^{-1})
$p(d_s)$	Soil particle size distribution
$p_f(d_s)$	Fully disturbed particle size distribution
$p_m(d_s)$	Minimally disturbed particle size distribution
P_w	Price of irrigation water (US$ m^{-3})
Q	Total saltating particles flux (kg m^{-2} s^{-1})
$q(d_s)$	Horizontal sand flux of particle size d_s (kg m^{-2} s^{-1})
ρ_b	Bulk soil density (kg m^{-3})
ρ_p	Particle density (kg m^{-3})
S	Crop subsidy (US$ ha^{-1})
σ_p	Ratio of free dust to aggregated dust
σ_j	Standard deviation of the jth mode
σ_m	The ratio between mass of impacting particle and mass ejected by bombardment
TGM	Total gross margin (US$)
u_*	Friction velocity (m s^{-1})
u_{*t}	Threshold friction velocity (m s^{-1})
W	Available annual water in each river basin (m^3 ha^{-1}).
w_j	Weight of the jth mode
X	Area under cultivation by each crop (ha)
Y	Seasonal irrigation demand (mm)

used for building resilience to climate change and mitigating human-induced threats to other declining saline lakes.

1. Introduction

Saline inland water bodies are a recurrent landscape feature of mid-latitude and subtropical closed hydrological basins (Hammer, 1986). With their current volume of 82,676 km^3, they account for 44% of the total lake water storage on earth (Messager et al., 2016). These lakes play an important role in determining regional climate patterns, sustaining biotic productivity and diversity, maintaining environmental and human health, and providing recreational services, minerals, and other resources (Hammer, 1986; Williams, 1996). Therefore the dynamics of saline lakes are of great importance to a broad array of stakeholders.

Over the past decades, several anthropogenic and climatic drivers have disturbed the hydrological balance of many inland saline lakes, often resulting in complete desiccation (Wurtsbaugh et al., 2017). Excessive evaporation with respect to the natural inflow (i.e. negative water balance), resulting from unrestricted withdrawals of surface and sub-surface water in the upstream watersheds and global warming, have decreased the water levels of most large saline lakes to an alarming extent across the world. Saline lakes' basins are mostly located in regions categorized as arid and semi-arid climates (Williams, 2002). Some examples of the declining saline lakes around the world are provided in Fig. 1. In most cases, unsustainable upstream water withdrawals have been a primary factor in the lake shrinkage (Williams, 1996). Lake Urmia, the Aral Sea, and Owens Lake are some examples of the shrinkage as a result of anthropogenic interventions. The Aral Sea faced a reduced area of 74% and volume of 90% as a result of basin-wide irrigation expansion (Micklin, 2007). Similarly, water use for human needs led to an average ~1.74 km^3 yr^{-1} reduction in water inflow to Lake Urmia from 1995 to 2010, resulting in ~86% decrease in the total lake volume (Chaudhari et al., 2018). Diversion of the supplying streams to meet agronomic and urban water demands desiccated California's Owens Lake completely by 1940 (Wurtsbaugh et al., 2017).

Comprehensive analyses of the trade-offs between ecological and economic benefits of the saline lakes are needed to identify sustainable options for managing these lakes, with the goal of restoring them while enabling economic activities in the surrounding regions (Wurtsbaugh et al., 2017). In addition to the loss of the above-mentioned ecosystem services, shoreline recession in theses saline lakes leaves salt-rich playas behind, which remain exposed to wind shear and are susceptible to aeolian transport of salt-rich dust. Snow melting in the surrounding mountains, soil salinization, vegetation degradation, poor air quality, and augmented risk of morbidity from respiratory diseases are some of the direct irreversible consequences of dust emissions from these desiccating lakes (Abuduwaili et al., 2010).

In response to concerns regarding the shrinking of saline lakes and the consequent impacts on the local environment, many ongoing national and sub-national efforts are aimed at increasing flows in upstream rivers. The endoreic nature of these basins makes

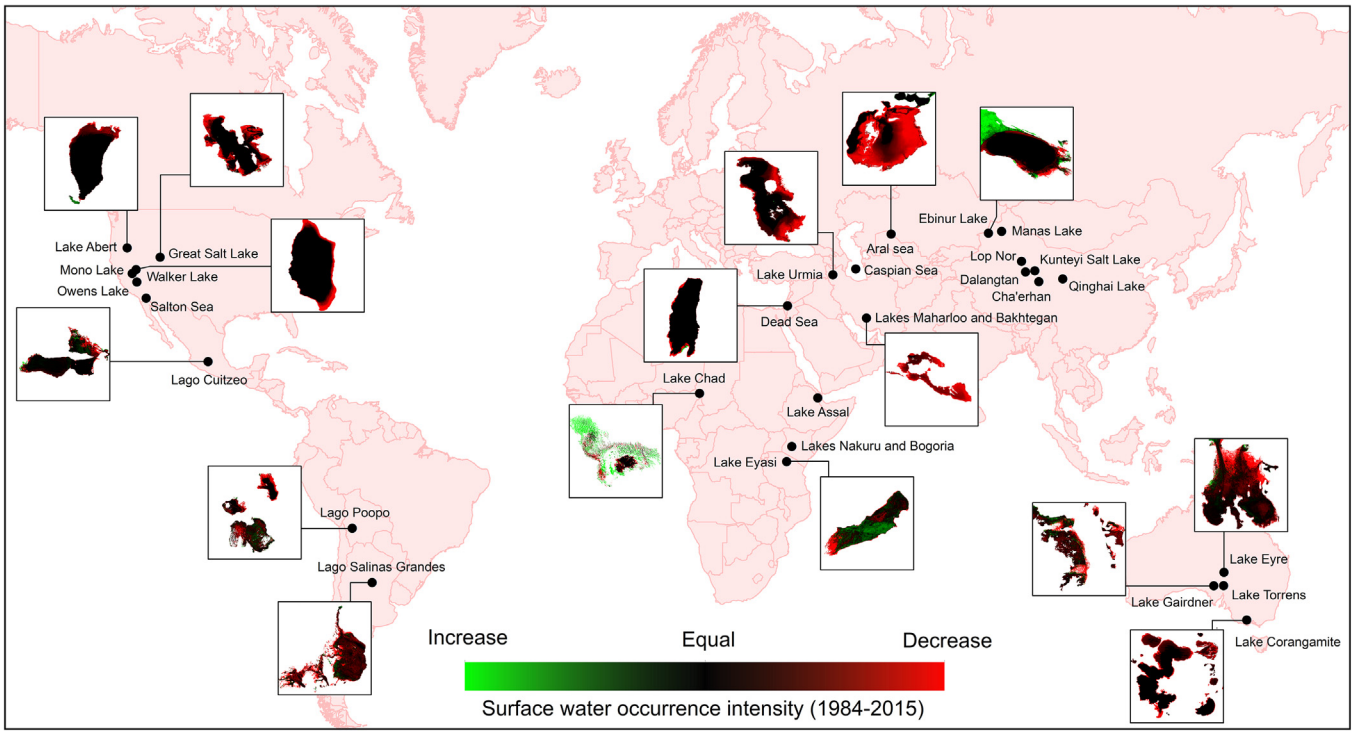

Fig. 1. Examples of the observed decrease in surface water area in major saline lakes around the world over the period 1984–2015 (Pekel et al., 2016).

them more vulnerable to changes in inflow regimes (Williams, 2002). Many approaches have been adopted by watershed managers to address the issue of saline lakes' shrinkage. One such approach is partial restoration of lakes by constructing physical barriers in the desiccated part, similar to the method used for the Aral Sea (Micklin, 2007). Another example is California's Mono Lake where the water inflows were increased by limiting withdrawals in the lake's upstream tributaries (Ryan, 2015). Multi-million to multi-billion-dollar projects for transferring water from the adjacent basins have been also considered as a method to preserve saline lakes, and examples include Lake Urmia, Dead Sea (Deatrick, 2016), and Utah's Great Salt Lake (Miller, 1987). In most cases, the required flow for restoration and preserving saline lakes can be provided by reducing water use, especially in the agricultural sector, although the projected climate change can help or exacerbate the management of the water demands (Wurtsbaugh et al., 2017). Despite utilizing various approaches for controlling the water withdrawals across saline-lake watersheds, a quantitative analysis of how agricultural land use would need to change to reduce water use, especially in face of future climatic uncertainties, is rare. Basin-wide technical and institutional improvements in the agricultural sector, reducing irrigated area, and cultivating less water-intensive crops can substantially conserve the water for restoring and preserving saline lakes. Hence, to assist policy makers and evaluate the priority for investment in land use and cropping pattern change, a comprehensive analysis of the land, climate, and the economy nexus of saline lakes' basins is needed.

To address this need, we propose a framework to guide evaluation of possible solutions based on land-use strategies that can facilitate restoration of saline lakes in the mid to long terms (2030–2050). The framework considers hydrological models combined with a salt balance to determine the water inflows that would be necessary to restore and keep the lake at the recommended level to maintain its ecosystem services. It also enables consideration of alternative cropping patterns to facilitate rehabilitation of lakes, especially in the context of projected climate change, while striving to protect farmers' income. As a results, it is possible to determine possible future hydrological, agronomic and socio-economic conditions in the lake's basin associated with an optimal land-use change strategy, aiming to reduce water consumption in the basin and restore the lake. Because such land-based interventions have the potential to increase greenhouse gas (GHG) emissions (Houghton, 2003; Smith, 2008), the framework also quantifies the emissions related to the recommended land-use change schemes. Although the lakes will differ and the specific analysis of each lake and its basin will require specific data, the proposed framework is generic and can be applied to similar saline-lake basins located in arid and semi-arid areas with unsustainable water withdrawals as a primary reason for decreased water flows into the lake. Some critical examples of these lakes are The Aral Sea, Great Salt Lake, Lake Urmia, Lake Abert, Walker Lake, Lake Poopó, and Owens Lake. If the basin-wide demographic, hydrological, climatic, and agronomic data for each river supplying the saline lake are available, the proposed framework can be applied for projecting the required adaptations in the agricultural land use. However, the proposed framework cannot be applied to lakes in arid regions where droughts and excess of evaporation relative to precipitation are the major causes of desiccation.

To mitigate the adverse consequences of lake recession in shorter time spans, the framework also enables consideration of partial restoration by identifying the part(s) of the lake that should be prioritized for restoration. This is based on the analysis of dust emissions from the lake bed since the dispersion of wind-blown saline dust from the playa, resulting from the desiccation of saline lake sediments, is the major concern for environmental and human health in nearby regions (Gillette et al., 1997). Here we prioritize the partial restoration option with the best potential for dust emission mitigation over other objectives, such as recreation or extraction of minerals. We quantify the potential for vertical emissions of saline dust from the lake bed in response to wind erosion to identify the zones with the higher priority for restoration.

The framework is detailed in the next section, followed by an illustrative application in Section 3.

2. Materials and methods

As illustrated in Fig. 2, the proposed framework comprises four steps. Step 1 involves projection of future climate conditions, depending on the targeted time horizon for restoration of the lake. This is commonly carried out by using outputs of global circulation models (GCMs). However, the variety of GCMs with different initial conditions and physics necessitates the application of multi-GCM ensemble for the basin under study to capture the uncertainties involved in the predictions of climate change. Therefore, this is taken into account in the framework as discussed in Section 3.

Step 2 requires establishment of a historical salt and water balance over the lake's area to relate limnological and hydrological processes of a saline lake to climatic and other long-term meteorological drivers. These hydrological processes can include the surface and sub-surface inflow or sediment transport dynamics. Among the climatic parameters related to the water balance of a saline lake, a reliable estimation of the evaporation rate is a challenge (Zilberman et al., 2017), especially if measured data are not available. At the same conditions, the evaporation from saline water bodies is different from freshwaters due to the different surface activity of brine (Lensky et al., 2005). Dissolved salts reduce the free energy of the water molecules, which influences the saturated vapor pressure depending on the salt concentration (Shokri-Kuehni et al., 2017a,b). This in turn modifies the evaporative fluxes. Therefore, relationships commonly used for estimations of the evaporation flux from freshwater cannot be applied for the case of saline lakes. Instead, estimation of the evaporation rate can be resolved by direct measurements, as in the present study and in Mor et al. (2018), or implementation of long-term mass balance models (e.g. Mohammed and Tarboton, 2012; Winter et al., 2003).

In step 3, the calibrated hydrological balance over the lake's area against system stressors provides the basis for estimation of the required inflow for restoration of the lake to the targeted water level for various time horizons. This will depend on how restoration is defined, what management objectives are preferred, and the constraints included. The restoration target level can be defined as the level that returns the degraded aquatic system to the conditions that are ecologically productive, protective, or aesthetically pleasing (Hobbs and Norton, 1996). It should be noted that the ecological target level for lake restoration is not a singular level and, in most cases, the ecological aspects are improved along

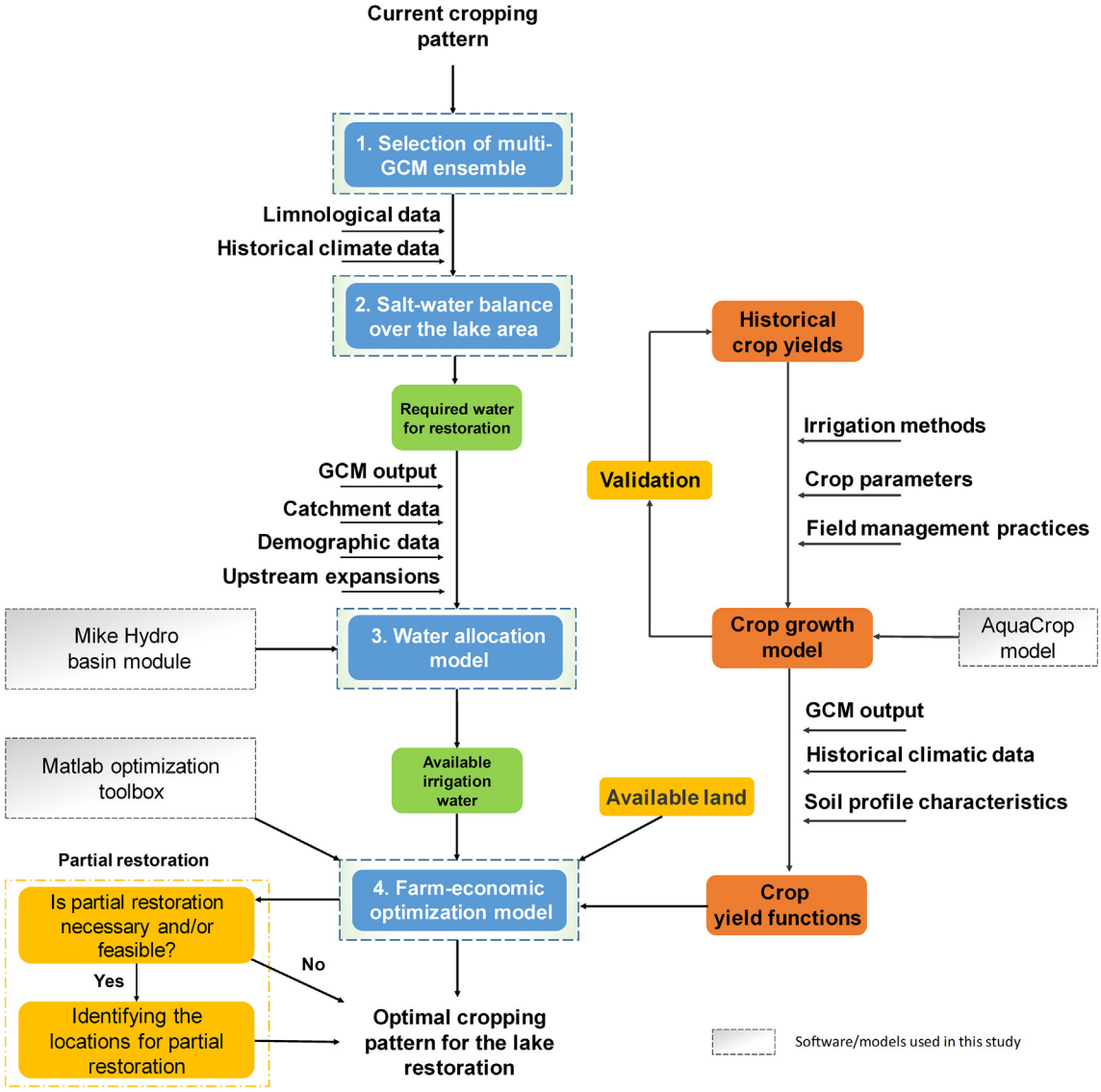

Fig. 2. The proposed framework for restoration of saline lakes (GCM: global circulation model).

a continuum of salinities and elevations. A vulnerability analysis of the ecological services provided by saline lakes to the water-level decline, descriptions of factors to which the saline aquatic system is sensitive, and quantification of trade-offs among various restoration objectives, can be the key elements in prioritizing and adopting a single elevation for the lake water. After the estimation of the required water, another model is needed to estimate the available water and allocate the remaining water (not used for restoration) among all stakeholders at the river basin scale. The water allocation approach needs to consider the future climatic, hydrological, agronomic, demographic and other drivers in a saline lake's basin.

Finally, step 4 aims at developing and evaluating alternative sustainable land-use and cropping patterns to reduce water usage in the agricultural sector that is needed for increasing the lake's water level. The focus is on agricultural usage because in most cases unsustainable development of agronomic activities in saline lakes' basins has been the major reason for the decline of lakes, including Lake Urmia (AghaKouchak et al., 2015; Chaudhari et al., 2018; Ghale et al., 2018; Hassanzadeh et al., 2012). We define a land use strategy as sustainable if it allows the inflow of required water to the lake over relevant management time scales while meeting the economic, social and environmental needs of the stakeholders in the basins. Water allocated to the agricultural sector (in step 3) becomes one of the inputs into a farm-economic optimization model to obtain the optimal cropping pattern at the river basin scale, subject to available irrigation water and land resources needed to restore the lake by the targeted time horizon. Estimation of the cultivated crop yields as a function of irrigation water in the supplying river basins provides another major input for the farm-economic optimization model (Fig. 2).

The system is then optimized to maximize income at the farm level for the new land use and cropping patterns. Other optimization objectives can also be defined, based on stakeholders' interests and data availability. As new cropping patterns involve land-use change, it is important to estimate the resulting change in GHG emissions, which is also included in the framework. The optimal agricultural water management solutions, identified through the optimization, enable decision and policy makers to evaluate how potential land-use schemes may perform, explore the interconnections between different system components, and identify the key factors affecting the restoration strategies. They can also consider various challenges, such as ensuring that farmers comply with recommended solutions, maintaining equity among stakeholders, behavioral and institutional barriers, and financing needed for the proposed land management policy. In case that coping with these challenges is not possible in the short term, consideration can be given to feasible partial restoration scenarios in parallel with the land-use optimization process. Depending on available resources and services provided by the saline lake, locations with the higher priority for restoration can be identified. The decision makers may also want to change the constraints or optimization objectives. Therefore, the proposed framework can be used as an iterative decision-support tool which can be updated as new information or alternative watershed resource management frameworks come to light.

The applicability of the proposed framework is illustrated in the next section through the case of the second largest (by volume) hyper-saline lake in the world – Lake Urmia in Iran – which is at risk of complete desiccation. Strategies for both partial and complete restoration are considered in the short (2030) and long terms (2050), respectively.

3. Application of the framework: the case of lake Urmia

The Urmia basin plays a pivotal role in Iranian national food supply. Nearly 10% of the country's agricultural area is located in the basin, producing about 6 Mt of crops annually. With an average annual precipitation close to 400 mm and average potential evapotranspiration of 530–680 mm, the basin's climate is classified as cold semi-arid (Kottek et al., 2006). The lake is located in a geological sink called graben where volcanic rocks caused by historical eruptions are widely distributed (JICA, 2016). The lake is terminal and surrounded by mountainous areas with elevations ranging from 1,270 to 4,000 m (mean sea level). It is supplied by 12 major streams flowing into the lake, with an average annual run-off ratio of 0.24 (JICA, 2016). The Talkhe and Zarineh rivers with the catchment areas of 12,717 and 11,838 km^2 compose 24.6% and 22.9% of the whole lake's basin area, respectively, while ~ 40% of the annual inflow to the lake is supplied by the Zarineh and Simineh rivers.

Construction of more than 44 reservoirs along the lake's tributaries (with the total storage capacity of ~1.413 km^3) and increasing the authorized groundwater withdrawals from 0.25 km^3 in 1980 to 1.6 km^3 in 2014, along with intermittent drought periods, doomed Lake Urmia to almost complete desiccation (Fathian et al., 2015; Jalili et al., 2016; Shadkam et al., 2016), which is unprecedented in the last 4,000 years (Kelts and Shahrabi, 1986). As a result, the lake lost 80% of its area and 96% of its volume in just 20 years, declining by 0.4 m yr^{-1} in the water level (Fig. 3). The growing in-field, modeling, and remote sensing evidence suggests that, although climate change and decreasing precipitation have exacerbated the decline of the water levels, intensified water withdrawal is one of the major reasons for the shrinkage of the lake (AghaKouchak et al., 2015; Chaudhari et al., 2018; Ghale et al., 2018; Hassanzadeh et al., 2012).

As mentioned earlier, airborne saline particles emitted from the desiccated parts of the lake, are a major concern for environmental and human health. Long-term fluctuations in hydrological and climatic parameters prevent an effective estimation of spatial distribution of the adjacent demographic and industrial centres exposed to the emissions. Hence, we evaluated the geo-spatial dispersion of PM_{10} (particulate matter $\leq$ 10um) emitted from the lake bed (Section 3.4.2.1) in the context of a five-hour storm that struck the Urmia basin in March 2018 at the mean wind speed of 44 km h^{-1} (gusts up to 70 km h^{-1}). The simulations were based on the assumption that the lake bed moisture was <5%. The HYSPLIT_4 (Hybrid Single-Particle Lagrangian Integrated Trajectory) model (Draxler, 1999; Rolph et al., 2017) was used to simulate the dispersion and deposition trajectories (particle speed deposition = 0.001 m s^{-1}). The emission rate was set equal to the vertical dust flux (F) as a function of wind speed, calculated from the vertical dust parameterizations explained in section 3.4.2.2. The spatial scattering range of the emitted saline fine particles as a result of the storm (Fig. 4a–c) suggests a very significant influence of dust from the desiccated parts of Lake Urmia on air concentrations of PM_{10} at the ground level (0–100 m above the surface).

Annual depositions of 13.03 Mt of sediments, 1 Mt of salt, and 1,076.45 Mt of herbicides, pesticides and fertilizers (WRMC, 2007), conveyed by inflowing rivers, dramatically exacerbate the environmental perils of wind-blown particulates. The composition of the deposited particles is of particular concern for human and animal health, as well as for vegetation. For example, chloride-containing airborne particles can lead to a range of metabolic and reproductive alterations to vegetation and respiratory-related threats for humans and livestock (McCune, 1991). Our analysis of the elemental composition of 49 near-surface sediments at the lake bed (initial geo-chemical data after Alipour et al., 2018) indicated significant contamination of deposits by arsenic and antimony and moderate contamination by rubidium and strontium (enrichment factors = 13.4, 11.9, 4.43, and 4.06, respectively).

Despite the emergence of the lake's recession between 2006 and 2014, the monetary incentives in agriculture and other sectors drawing on the water in the lake's basin hindered its conservation

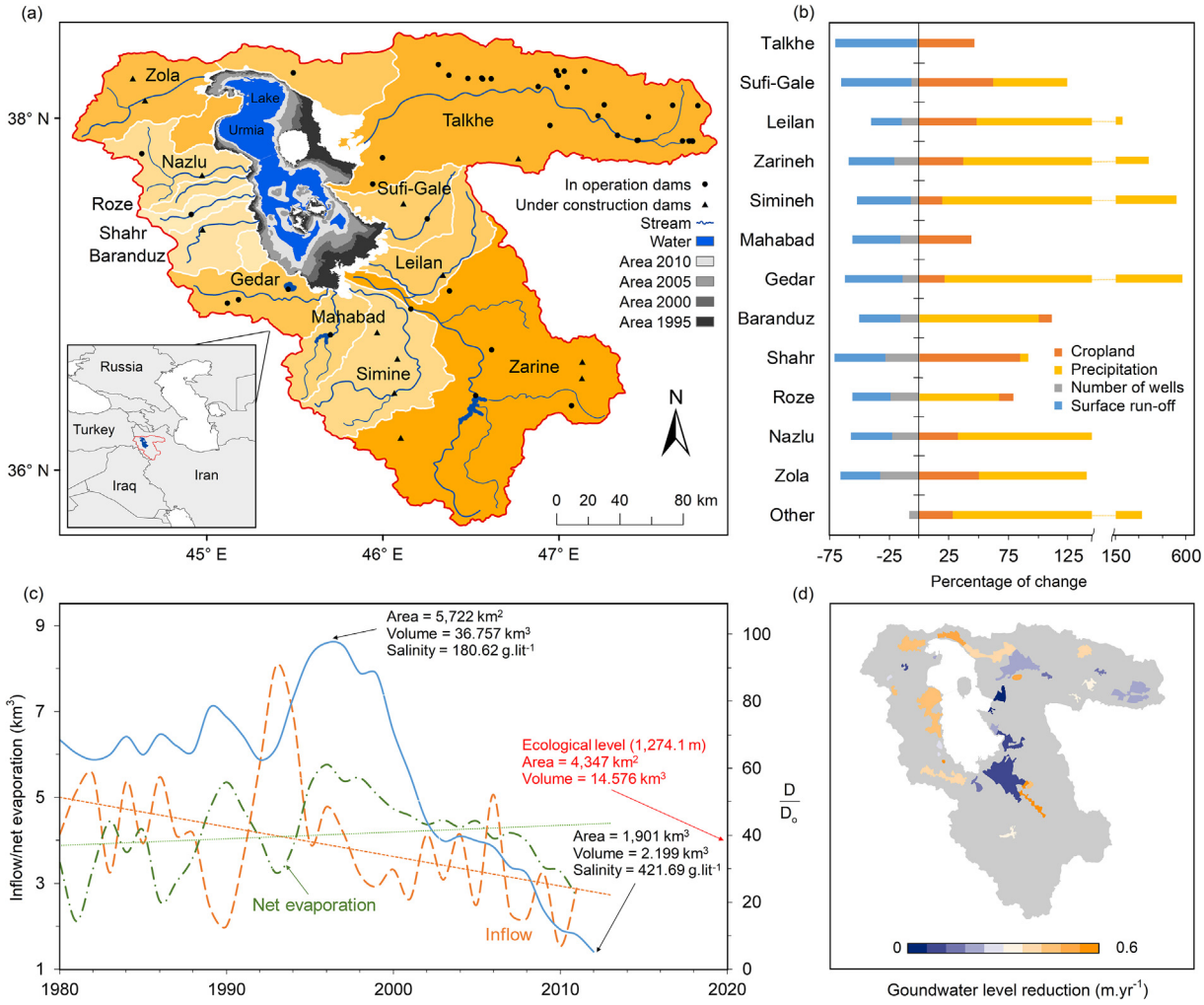

Fig. 3. a. Lake Urmia's watershed and the river basins of its tributaries. b. Increase in the number of wells, decrease in precipitation, reduction in surface run-off, and increase in the area under cultivation in each river basin. The increase in the number of wells is obtained through comparison of two periods: before 1985 and from 1985 to 2001. For the surface run-off, average river discharges in the 1975–1995 and 1995–2011 periods are compared. The decrease in the annual precipitation in each basin is acquired through comparison of the 1980s and 2000s. Land-use change is for the period 1987–2007. c. Annual water stocks and flows determining Lake Urmia's hydrological balance. For the period between 1980 and 1995, the difference between the inflow to the lake and net evaporation (evaporation minus precipitation on the lake's surface) was negligible; since 1995, the gap between the inflow and outflow from the lake has grown steadily. d. Annual decrease in the groundwater table level between 2004 and 2014.

(Madani, 2014). In 2014, the near-complete desiccation, with the water level declining to 1,270.1 m, received significant scientific and public attention (AghaKouchak et al., 2015; Garousi et al., 2013). As a consequence, the Iranian government and the UN issued a US$ 1.3 bn plan for rehabilitation of the lake and surrounding wetlands which saved the lake from complete desiccation. However, in the first four years of this ten-year restoration plan, the lake level increased by only 0.6 m to 1,270.7 m, corresponding to an increase in water volume of 525 Mm^3. This falls well below the targeted ecological level established by the Lake Urmia Restoration Committee of 1,274.1 m. This ecological target reflects the lake level and volume at which salinity is expected to fall below 240 $g\,l^{-1}$ NaCl. This salinity represents the maximum tolerance level for brine shrimp, the only fauna at the top of the ecological pyramid of the lake (Abbaspour and Nazaridoust, 2007). Our calculations showed that an additional water volume of 11,850 Mm^3 is required to achieve the target water level of 1,274.1 m (based on the lake level-area-volume relationships; see section SI.1 in the Supplementary Information (SI) for details).

To meet the water needs for short-term recovery of the lake (ten years), *trans*-basin water diversions were implemented by government as a part of the rehabilitation plan. One of these is a US$ 100 million tunnel (35.7 km) which will be used to transfer 0.64 km^3 of water per year from the adjacent basin (the lower Zab, one of the Tigris's tributaries). However, desertification and degradation of the Tigris's downstream marshes as a result of this water diversion, dam construction on other transboundary tributaries, and plans by Turkey and Iraq for impoundment of 34 km^3 of Tigris's water (Altinbilek, 2004) cast serious doubts on the long-term efficacy of the solutions related to inter-basin diversion. Moreover, occurrence of 33 dust events per year in southwestern Iran, with hourly PM_{10} concentrations above 500 $\mu g\,m^{-3}$ might be attributed to a 65% decrease in Tigris's historical discharge and desiccation of its deltaic wetlands compared to the historical values in the period 1931–1952 (Rahi and Halihan, 2018).

The following sections detail the framework steps as applied to the case study.

3.1. Step 1: selection of multi-GCM ensemble

Required climatic parameters for projecting the future hydrological and agronomic conditions in the Urmia basin for the period 2020–2050 were obtained using an ensemble of GCMs from the IPCC's Fifth Assessment Report (Emori et al., 2016). The outputs

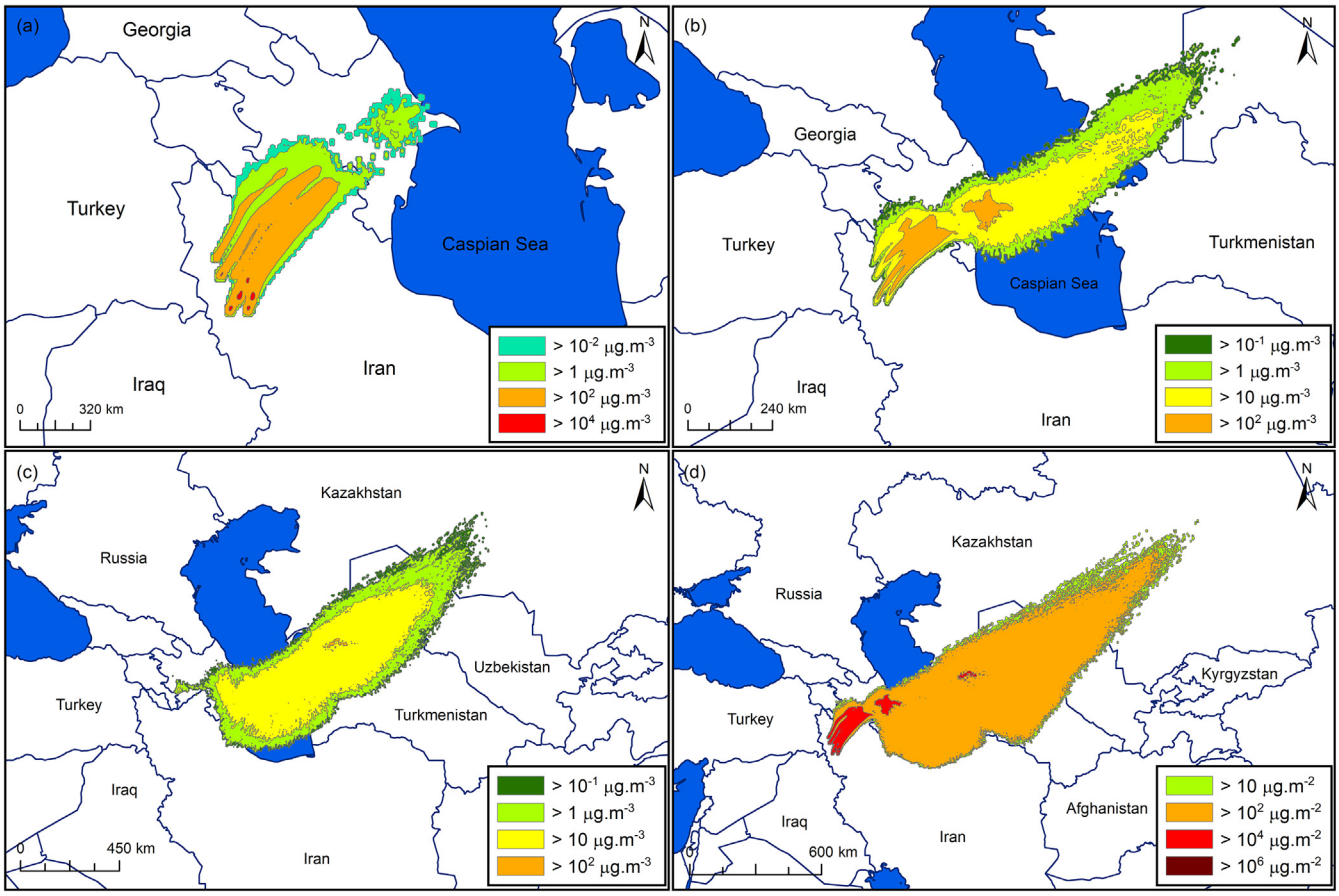

Fig. 4. a, b, and c. Average concentrations of PM_{10} (particulate matter $\leq$ 10um) between the surface and 100 m above ground level after 6, 12, and 18 h from the beginning of the storm, respectively. d. Aggregate PM_{10} disposition rate 24 h after the start of the simulation. The model simulates the PM_{10} dispersion originated from the Lake Urmia's saline playa (in a hypothesized case of the lake's desiccation) during a dust storm on 24/3/2018 (14:00 UTC). A mean of 27 ensemble members (offset is one meteorological grid point in the horizontal and 0.01 sigma units in the vertical direction) was calculated for the 18-hour dispersion simulation. For further details, see section SI.2 in the Supplementary Information).

of the 16 GCMs under two Representative Concentration Pathways (RCP) forcing scenarios (4.5 and 8.5) were considered to capture the uncertainties in the projected climates. Including different realizations of the GCMs, a total of 34 and 25 ensemble members were used for RCP 4.5 and 8.5, respectively. Details of the GCMs and their used realizations are provided in Table 1. They were statistically bias-corrected over the reference period of 1960–1995, i.e. before the lake's desiccation. The bias-corrections were based on Eq. (2) in Hawkins et al. (2013) using high-resolution gridded time-series dataset for observed climatic parameters at 0.5° resolution, based on Harris et al. (2014), version CRU TS 4.02. This method was selected as it is computationally more efficient than more advanced techniques because of the large number of ensemble members.

Table 1
Global circulation models (GCMs) used in this study for projecting future (2020–2050) hydrological and climatic conditions in the Urmia basin.

GCM	Used realizations under RCP 4.5[a]	Used realizations under RCP 8.5[a]	Spatial resolution (latitude × longitude; degrees)	Centre (Country)
ACCESS1-0	1	1	1.25 × 1.87	CSIRO-BOM (Australia)
CNRM-CM5	1	1	1.40 × 1.40	CNRM-CERFACS (France)
GFDL-CM3	1	1	2 × 2.5	NOAA (USA)
GFDL-ESM2G	1	1	2.02 × 2	NOAA (USA)
GFDL-ESM2M	1	1	2.02 × 2.5	NOAA (USA)
GISS-E2-H	1,2,3,4,5	1,2	2 × 2.5	NASA (USA)
GISS-E2-R	1,2,3,4,5	1,2	2 × 2.5	NASA (USA)
GISS-E2-R-CC	1	1	2 × 2.5	NASA (USA)
HadGEM2-CC	1	1	1.25 × 1.87	MOHC (UK)
HadGEM2-ES	1,2,3,4	2,3,4	1.25 × 1.87	INPE (Brazil)
IPSL-CM5A-LR	1,2,3,4	1,2,3,4	1.89 × 3.75	IPSL (France)
IPSL-CM5A-MR	1	1	1.26 × 2.5	IPSL (France)
IPSL-CM5B-LR	1	1	1.89 × 3.75	IPS (France)
MPI-ESM-LR	1,2,3	1,2,3	1.86 × 1.87	MPI (Germany)
MPI-ESM-MR	1,2,3	1	1.86 × 1.87	MPI (Germany)
NorESM1-M	1	1	1.89 × 2.5	NCC, NMI (Norway)

[a] Realization number indicates the initial conditions of the ensemble member.

3.2. Step 2: salt-water balance over the lake's area

To plan for a sustainable restoration of a lake, the primary question is: how much water is required annually by each supplying tributary to restore the lake in the face of future hydrological, agronomic, and climatic conditions? To estimate the required inflow for the Lake Urmia, we established a hydrological model over the lake, combined with a salt balance. For simplicity, here we adhered to the recommended target level adopted by the Restoration Committee (1,274.1 m) because it is expected that above this water level the lake's water salinity would fall below the maximum salinity that could be tolerated by brine shrimp (240 g l^{-1} NaCl).

Unlike previous analyses of the water balance over the lake and its tributaries' watershed (JICA, 2016), here we accounted for the effect of projected climate change. Moreover, most of the existing models did not consider the effect of dissolved salt mass on the water balance and the variations in the depth of the lake, which were accounted for in the present study. The lake's hydrological balance was used to estimate the total annual and sub-surface inflow to the lake as well as the salt precipitation rate. The water needed for restoration of the lake under different scenarios (partial or complete restoration) was calculated based on this reconstruction of the hydrological balance. The hydrological model was first calibrated against the climatic parameters and the surface water input in the reference period, here taken to cover the period from 1996 to 2010 due to limited data availability. Then, using the calibrated model, the amount of water required for rehabilitation to the target ecological water level for different time and climate scenarios was estimated. This is discussed in more detail next.

3.2.1. Water and salt mass balance in the reference period (1996–2010)

In this step, the lake's mass balance, including both the mass of water and dissolved salt, was established first. Subsequently, the meteorological and bathymetry data over the period were implemented to calibrate the model parameters. The change in the mass of the brine (m) after a period Δt was determined as follows (Lensky et al., 2005):

$$\frac{\Delta m}{\Delta t} = -m_{evaporation} - m_{salt} + m_{\inf} + m_{pre} \quad (1)$$

In Eq. (1), $m_{evaporation}$ is the mass of evaporated water according to the lake's area, m_{salt} is the change in the mass of salt available in the water, m_{inf} is the amount of water that enters the lake during a particular time period, and m_{pre} is the mass of precipitation over the lake's area. The change in the mass of salt, m_{salt}, can be positive or negative, depending on the deposition or dissolution of salt in water. It was calculated as:

$$m_{salt} = m_{saltavailable} + m_{saltrivers} - m_{saltnew} \quad (2)$$

where $m_{saltavailabe}$ and $m_{saltnew}$ represent respectively the total amount of salt present in the lake at the beginning and the end of a particular time span and can be obtained directly by measuring the concentrations of salt in the lake; $m_{saltrivers}$ is the amount of salt added to the lake by its rivers (Table 2). If m_{salt} is positive in a particular year, it means that the salt is precipitated on the lake bed and vice versa. The bathymetry data from 2010 were used to calculate the area, level, and volume of the lake, using ArcGIS surface volume tool. The volume of salt added to or removed from the lake at each time (assuming the salt deposition is related to the halite whose density is 2,160 kg m^{-3}) was taken into account to update the estimated area, level, and volume of the lake. However, the lake bed surface area (i.e. 3D surface) was assumed to be constant. The observed precipitation over the lake's region and its corresponding area during 1996–2010 was adopted from JICA (2016).

Table 2
Salinity and average mass of salt added to the lake by different rivers during 1996–2010.

River	Average annual inflow to the lake (Mm^3)	Total dissolved solids (mg l^{-1})	Average amount of added salt (t yr^{-1})
Barandooz chay	174.5	288.282	50,322.89
Roze chay	25.8	437.526	11,294.58
Gedar chay	202.8	324.738	65,882.62
Nazlu chay	137.4	264.865	36,393.63
Shahr chay	51.1	403.800	20,673.75
Mahabad chay	118.1	436.872	51,623.41
Simineh rood	296.7	260.304	77,237.22
Zarineh rood	879.9	302.022	265,770.50
Zola chay	27.8	662.304	18,440.75
Sinikh chay	17.3	357.956	6218.88
Ghale chay	27.5	339.060	9,348.78
Azar shahr	22.6	145.000	3,279.03
Mardoogh chay	60.4	250.000	15,111.33
Lilan chay	42.7	287.850	12,300.79
Javan chay	7.9	250.000	1,988.50
Soofi chay	30.4	286.851	8,755.05
Aji chay	166.4	8,863.020	1,475,385.57
Surrounding plains	316.4	150.000	47,467.05

No data were available on the evaporation rates from the lake's surface. Therefore, the annual rate of evaporation was estimated based on pan evaporation data. While it is not possible to use pan evaporation values directly to calculate the evaporation from open water bodies like a lake, a correction factor is typically used, here assumed at 0.77 (Darvishi, 2014). To account for the presence of dissolved salts, we applied two different methods for correction of the freshwater pan evaporation data. In both methods, a time series of pan evaporation between 1996 and 2010 was applied, including the average of annual freshwater pan evaporation measured experimentally at ten different stations around the lake and the only station within the lake.

In the first method, the ratio between lake water pan evaporation (e_s) and average freshwater pan evaporation (e_f) in each year was used as a factor for correcting the average of freshwater pan evaporation values. In other words, the annual evaporation from the lake's surface was calculated as $e_f \times (es/e_f)$. In the second method, saline water evaporation rate from the lake was assumed to be constant at 1,200 mm yr^{-1} (JICA, 2016). This value was calculated by establishing a water balance over the lake's area as:

Water balance = (Surface water inflow)
+ (Groundwater inflow : Groundwater recharge
+ Water from groundwater storage)
− (Base flows of the rivers)
+ (Precipitation over the lake)
− (Evaporation from the lake)
− (Water uptake from surface water and groundwater

Ten different cases of annual evaporation rates from the lake's surface were used for the annual water balance calculation. They ranged from 1,000 to 1,900 mm yr^{-1} with a 100 mm yr^{-1} interval, referring to the average annual freshwater pan evaporation value at stations adjacent to the lake, equal to 1,611 mm (obtained via the Thiessen method (Thiessen, 1911)). The case with the evaporation rate of 1,200 mm yr^{-1} showed the highest correlation between the annual average lake water level and accumulated annual water balance. Using the total precipitation over the lake and the above two methods for estimation of the evaporation rate, net annual inflows to the lake were calculated as the sum of surface and sub-surface inflows.

Table 3
Fresh water and brine evaporation before and after application of salt and lake constants correction.

Year	Average of ten stations (freshwater) (mm)	Golmankhan station (freshwater) (mm)	Golmankhan station (saline) (mm)	Saline to freshwater ratio	Evaporated water from the lake calculated by JICA (Mm^3)	Average of ten stations modified for salt presence × saline-to-freshwater ratio (mm)	Golmankhan station modification (×0.77) (mm)	Average of ten stations (freshwater) modified for salt presence × 0.77 (mm)
1996	1,424.7	1,385.1	1,191.5	0.86	6,864.5	1,225.5	917.4	943.7
1997	1,370.9	1,181.7	918.9	0.77	6,814.8	1,066.0	707.5	820.8
1998	1,473.3	1,386.0	1,098.3	0.79	6,686.9	1,167.4	845.6	898.9
1999	1,417.2	1,168.2	1,116.0	0.95	6,311.6	1,353.8	859.3	1,042.4
2000	1,503.7	1,385.9	997.7	0.71	5,900.7	1,082.5	768.2	833.5
2001	1,615.4	1,489.3	1,391.1	0.93	5,476.6	1,508.9	1,071.1	1,161.8
2002	1,505.7	1,381.9	1,115.6	0.80	5,266.2	1,215.5	859.0	935.9
2003	1,406.0	1,557.3	1,153.6	0.74	5,241.6	1,041.5	888.2	801.9
2004	1,433.9	1,433.5	1,248.6	0.87	5,319.9	1,248.9	961.4	961.7
2005	1,515.4	1,338.8	1,205.7	0.90	5,138.9	1,364.7	928.3	1,050.8
2006	1,484.5	1,267.6	1,181.4	0.93	5,108.5	1,383.5	909.6	1,065.3
2007	1,383.0	1,164.3	1,115.9	0.95	4,929.1	1,325.5	859.2	1,020.6
2008	1,636.7	1,687.0	1,452.7	0.86	4,565.0	1,409.4	1,118.5	1,085.2
2009	1,378.9	1,379.2	801.8	0.58	4,409.4	801.6	617.3	617.2
2010	1,430.0	1,265.1	1,070.9	0.84	4,069.6	1,210.5	824.5	932.1
Average	1,465.3	1,364.7	1,137.3	0.82		1,205.5	863.8	928.2

Two other methods were also applied to calculate the annual evaporation from the lake (see Table 3): 1. correction of the evaporation values obtained in the first method described above by multiplying with the lake-effect correction factor (0.77); and 2. modification of the saline water pan evaporation values using the lake-effect correction factor. However, the calculated total annual inflow into the lake using these methods was not acceptable since the estimated values for the total inflow to the lake were lower than the total surface entry, measured by the discharge gauges at the periphery of the lake (~2,600 $Mm^3\ yr^{-1}$).

Although the aforementioned mass balance enabled us to estimate the total inflow and the under-surface water gain, there was still a need for updated relationships between the lake's level, area, and volume, which also consider the salt precipitated on the lake bed to determine the required water for restoration. We initially used the bathymetry data from the year 2010 to predict the lake's area and volume as a function of the lake's level (Section SI.1 in the SI) and also the lake's level as a function of its volume, i.e. $Level = a_c \times (Volume)^{b_c} + c_c$. The constant parameters (a_c, b_c, and c_c) in this relationship were chosen as the calibrating parameters. The total annual inflow results obtained through the combined water and salt balances enabled us to calibrate these relationships. These sets of fitted functions and the calibrated lake level-volume relationships were then used to predict the required water for the restoration of the lake between 2020 and 2050.

We used Monte Carlo simulations to address the issue of the equi-finality and parameter uncertainty in the calibration process. We investigated the calibration of the three parameters (a_c, b_c, and c_c) ranging from 2.189×10^{-5} to 5.189×10^{-5}, 0.50 to 0.52, and 1,267 to 1,269, respectively. A 1000 combinations of the calibrating parameters were derived employing uniform sampling strategy from each parameter within the above range. We then estimated the annual total inflow between 1999 and 2010 using the first evaporation method (preferred because the second method assumes a constant annual evaporation rate), precipitation data and the water balance over the lake's area. We finally compared these results with the total inflow calculated for the same period by considering both the water and salt balances. A coefficient of determination (R^2) between the two computed ranges of the total annual inflow equal was set at 0.6 as an acceptable threshold for choosing a set of calibration parameters.

3.2.2. Mass balance in the period 2020–2050

The calibrated level-volume relationship was then used to estimate the required annual surface water inflows for complete restoration of the lake to the target water level (1,274.1 m) by 2050. For the whole lake, the calculations of the amount of salt added to the lake by its rivers demonstrated that the volume of added salt was negligible compared to the volume of lake: the average total volume of added salt was close to 1 $Mm^3\ yr^{-1}$, compared to the surface water inflow of 2,606.5 $Mm^3\ yr^{-1}$. Hence, in the established hydrological cycle between 2020 and 2050, the salt balance was omitted. This was also because the amount of salt which dissolves from the lake bed into the water cannot be estimated precisely. Owing to a large difference between historical observations and the model output, bias-corrected precipitation and evaporation rates projected by the GCMs were utilized to estimate the evaporation and precipitation over the lake's corresponding area in each year in the period. The rainfall and evaporation time series from each GCM were bias-corrected as mentioned earlier (based on Hawkins et al. (2013)), using the observed precipitation data at synoptic stations adopted from Harris et al. (2014) and the evaporation rates calculated in Section 3.2.1, respectively. The reference period for the bias-correction of the rainfall time series was arbitrarily chosen to be between 1960 and 1995. This period was long enough to cover inter-annual climatic variabilities before and after the lake's shrinkage. The annual inflow volumes required to attain the target level of 1,274.1 m by 2050 were estimated using the calibrated level-volume relationship discussed in Section 3.2.1. Considering the annual water gain by the lake from precipitation and projected evaporation, we calculated how much water is required annually to refill the lake to the target level by 2050. The calculations were repeated for each multi-GCM ensemble member over the acceptable sets of calibration parameters to determine the uncertainty ranges for the required volume. Finally, the annual inflow required for the restoration was distributed across the tributaries proportionally to the discharge history of each river. The estimated water requirement for each river was then used as an input for the water allocation model in step 3 of the framework.

3.3. Step 3: water allocation model

To capture the variabilities and uncertainties of GCM-based predictions of the future climatic and hydrological conditions in the Urmia basin, the water allocation modelling and optimization (step 4) were based on a mean of the multi-GCMs with 34 ensemble members for the RCP 4.5 scenario and 26 members for RCP 8.5. All the required climatic parameters were computed as an ensemble mean with equal weighting of each ensemble member. The

final annual water requirement for restoration of the lake by 2050 was set as the mean of both multi-parameter and multi-GCM ensemble predictions under RCP 4.5 and RCP 8.5 (i.e. 3,648 and 3,692 $Mm^3\ yr^{-1}$, respectively).

We calculated the available runoff and the increase in water demand to meet the lake's inflow target at the river-basin scale and then prioritized the latter to achieve the aims of the land-based restoration plan. In each watershed, the remaining water (the difference between available runoff and lake inflow requirement to meet the restoration target) was distributed among the industrial, municipal, and agricultural sectors, leading to an estimate of the maximum water available for irrigation after the distribution.

The water-resources management model in the Mike HYDRO Basin module (Mike, 2017) was used for the allocation of water within each river basin. The total projected allocation of the annual run-off to water users, hydropower plants, and reservoirs was prioritized by the global ranking algorithm implemented in the model. The highest global priority was assigned to the municipal and industrial water users, while irrigation water users were assumed to have lower priority because of the lower economic productivity of water in agriculture. The discharge at the river inlet into the lake was set equal to the annual required flow for lake restoration. The yearly surface water run-off in each tributary catchment and sub-catchment was estimated as a product of precipitation and the run-off ratio, using the average of the multi-GCM bias-corrected precipitations between 2020 and 2050, and calibrated historical run-off ratios extracted from Table 2.6.3 in JICA (2016). Annual run-off ratios were calculated utilizing observed precipitation data (provided by Iran's Water Resources Management Company) and recorded surface discharge at the neighboring end points of the supplying river basins. The accuracy of the runoff ratios for each basin was checked by calculation of the runoff depth (annual discharge divided by the catchment area) for each river. The average runoff depth for the supplying rivers was 318.6 mm, with Mahabad, Shahr, and Talkhe having the highest runoff depths of 699.9, 472.7, and 419.9 mm, respectively (Table 2.6.4 in JICA, 2016).

There are no complete data on the proportion of the municipal water that is returned back as grey water or how much urban water is consumed. Equally, data on future projections do not exist. Therefore, the time series of the municipal and industrial water usage per capita and the increase in the number of residents in each river basin (see WRMC, 2007 for details) were applied to predict the non-irrigation water demand until 2050. It was assumed that the current urban per-capita water is consumed completely and there is no return (as grey water) to the network. The expected annual outflow (evaporation and agricultural water supply) from each reservoir under construction was also accounted for as additional water. The outputs from this part of the framework were fed into the optimization model as the maximum available water for irrigation, as discussed in the next section.

3.4. Step 4: farm-economic optimization

This step aims to identify optimal solutions for a full or partial restoration of the lake. It involves basin-scale optimization of land use and cropping patterns subject to water availability, while protecting farmers' income. The latter is used as the objective function, as follows (García-Vila and Fereres, 2012):

$$TGM = \sum_{i=1}^{N}[(P_{ci} \times X_i \times F_i(Y_i) + S_i \times X_i)] - (C_{ai} \times X_i + P_{wi} \times Y_i \times X_i \times 10)] \quad (3)$$

where TGM is the total gross margin (US$), i represents each crop analyzed (1,2,...,N), X is the area under cultivation (ha), Y is the seasonal irrigation demand (mm), $F(Y)$ is the crop-yield production function ($t\ ha^{-1}$), P_c is the income received by farmers ($US\$\ t^{-1}$), S is the crop subsidy ($US\$\ ha^{-1}$), P_w is the price of irrigation water ($US\$\ m^{-3}$), C_a is the production cost ($US\$\ ha^{-1}$) and 10 is the units conversion factor.

The optimization is subject to the constraints on the available cropping lands and irrigation water:

$$\sum_{i=1}^{N} X_i \leqslant A \quad (4)$$

$$\sum_{i=1}^{N}(X_i \times Y_i \times 10) \leqslant A \times W \quad (5)$$

where A represents the total area under cultivation in each river basin, and W is the available annual water in each river basin ($m^3\ ha^{-1}$).

The model was optimized using Matlab Optimization Toolbox™ (Mathworks) and applying the 'fmincon' function. As this function minimizes rather than maximizes, the inverse of the objective function (*1/TGM*) was used and optimization carried out for each year between 2020 and 2050, subject to the above constraints. The final optimal cropping pattern and land use for agriculture were estimated as an average of the optimal land use and cropping pattern calculated for each year. It should be noted that the optimization model does not account for all the counter-measure projects employed by the Iranian government, such as facilitating the effluent transfer to the lake (for a complete list of these, see WRMC (2007)).

The various inputs into the optimization model, shown in Fig. 2, are discussed below.

3.4.1. Crop-yield functions

One of the inputs required for the optimization is an estimate of the variations in crop yields with applied irrigation water in face of projected climatic conditions. The AquaCrop model (Raes et al., 2009; Steduto et al., 2009) was used for this purpose to determine the crop-yield responses ($F(Y)$ in Eq. (3)) to climatic and irrigation variability and to develop crop-water production functions. The following major cultivated crops in the Urmia basin were considered: winter wheat, barely, maize (grain), sugar beet, oilseeds, potato, tomato, cucumber, water melons, alfalfa, dry beans, apple, pear, and stone fruits. Their yield responses were analyzed to determine the crop yield as a function of available irrigation water and other environmental factors. In addition, pistachio was selected as one of the alternative crops for cultivation as it has a lower irrigation demand and higher market value (also proposed by the Restoration Committee). Cultivar-specific crop parameters, including the time needed to reach the maximum canopy cover (CCx), canopy senescence, physiological maturity and flowering (or the start of yield formation) were adopted from Table 11 in Allen et al. (2005). This source was also used to obtain the average maximum effective rooting depth (Table 22 in Allen et al.). The average planting density, planting method (direct sowing or transplanting) and use of fertilizers were the field and management parameters tuned by the historical crop yields. Historical crop yields (FAO, 2016) were compared with simulated crop yields to validate the AquaCrop model against field and irrigation management practices. Regression techniques were then applied to obtain the yield response function for each crop for the period 2020–2050. For other cultivated crops and where input data for AquaCrop model parameterization were missing, the average annual potential evapotranspiration was assumed at 700 mm. The latter was calculated using the Hamon method based on monthly data of three weather stations (JICA, 2016).

Based on the soil map of the Urmia basin (Hengl et al., 2017), the soil type in this area can be categorized as Inceptisol (Service USDoASC, 1999). The soil moisture profile for each region was acquired from ERA-Interim reanalysis. Daily rainfall (mm) and climate time-series data, including daily relative humidity, minimum and maximum temperature (°C), and wind speed (m/s) between 2020 and 2050 were obtained by taking an average from the bias-corrected output of the multi-GCM ensemble. As mentioned earlier, the climate time series were bias-corrected according to Hawkins et al. (2013) using the updated data from Harris et al. (2014).

3.4.2. Partial restoration and land use optimization in the agricultural sector

As mentioned earlier, the optimization model allows provision of the required water for restoration of the lake. However, in some cases, attaining the optimal land use and cropping patterns may not be viable in a short term. Accordingly, feasible partial restoration solutions in parallel with the agricultural land use optimization would be beneficial to mitigating the adverse consequences of the lake's shrinkage. If partial restoration is needed and feasible, it is important to determine the parts of the lake that should be prioritized for restoration. This will depend on many factors, such as agriculture, extraction of minerals from the lake bed or recreational activities. Here we focus on the avoidance of dust emissions from the dried lake bed due to their adverse impacts on human health, animals and vegetation. The following sections provide an overview of the dust emission sources and the methodology used to estimate the geo-spatial dispersion of PM_{10} through vertical dust parameterization mentioned previously in Section 3 and Fig. 4.

3.4.2.1. Identification of dust emission sources. Locations vulnerable to wind erosion were characterized through the daily Aerosol Optical Thickness (AOT) obtained by Moderate Resolution Imaging Spectroradiometer (MODIS)/Terra dataset (5 Min L2 Swath, 3 km resolution at nadir, both over land and ocean, MOD04_3K) over the lake's area between 2010 and 2016 (Levy and Hsu, 2015). We chose this period because the lake had the lowest water level between 2010 and 2015. For each pixel, the average of daily AOT intensities was multiplied by the number of days which had the measured AOT values >0.15 (intensity × frequency) to obtain an index for each pixel, here called 'aerosol intensity-frequency'. The pixels with an aerosol intensity-frequency index value higher than the 75-percentile of the calculated indices for all pixels between 2010 and 2016 were identified as dust sources within the lake's domain. These sites were mostly located on the lake's islands and on the margins of the southern half of the lake. The sediment at the lake's periphery can be classified as sandy loam and silty clay loam-textured, except the Jebel site on the west shore which has sand dunes (Table 4).

Table 4
Sediment composition of 12 sites on the margin of Lake Urmia. Soil textures in Fig. 9 are based on these compositions.

Site	Sand (%)	Silt (%)	Clay (%)
1	4.7	77.5	17.7
2	8.4	75.2	16.3
3	22.9	60.2	16.9
4	42.0	45.0	13.0
5	4.3	78.7	17.0
6	30.5	57.0	12.5
7	31.0	56.0	13.0
8	46.0	42.0	12.0
9	43.0	49.0	8.0
10	7.0	76.0	17.0
11	4.0	66.0	30.0
12	73.0	18.0	9.0

3.4.2.2. Vertical dust parameterization. Two parameters should be determined first in estimations of the vertical dust flux: 1. the threshold friction velocity at which the soil particles start to move; and 2. the horizontal saltation flux (Kang et al., 2011). Threshold friction velocity (u_{*t}) is defined as the minimum friction velocity required for the commencement of soil-particles movement and the saltation process. Here, the relationship proposed by Shao and Lu (2000) was used to calculate the threshold friction velocity. For a particle with diameter d_s, six formulations were used to determine the horizontal sand flux, $q(d_s)$ (kg m^{-2} s^{-1}). Details of those equations can be found in White (1979), Kawamura (1951), Owen (1964), Sørensen (2004), Lettau and Lettau (1978), and Durán et al. (2011). Aggregate flux intensity, Q, of saltating particles of all sizes was then estimated as follows (Shao et al., 2002):

$$Q = \int_{d_1}^{d_2} q(d_s)p(d_s)\delta ds \tag{6}$$

where d_1 and d_2 are the lower and upper saltating particle size limits, respectively, and $p(d_s)$ is the soil particle size distribution. Shao (2001) assumed $p(d_s)$ as a combination of two idealized particle size distributions, known as minimally disturbed particle size distribution $p_m(d_s)$, and fully disturbed particle size distribution $p_f(d_s)$. During weak erosion, $p(d_s)$ is close to $p_m(d_s)$, while when the erosion is strong, $p(d_s)$ is close to $p_f(d_s)$. Shao (2001) represented $p(d_s)$ as:

$$p(d_s) = \omega p_m(d_s) + (1-\omega)p_f(d_s) \tag{7}$$

and

$$\omega = \exp(-(u_* - u_{*t})^3) \tag{8}$$

where u_* is the friction velocity and u_{*t} is the threshold friction velocity. The minimally and fully disturbed particle size distributions can be deemed as the sum of lognormal distributions, i.e.:

$$p_{m,f}(d_s) = \frac{1}{d_s}\sum_{j=1}^{J}\frac{w_j}{\sqrt{2\pi}\ln\sigma_j}\exp\left(-\frac{(\ln d_s - \ln D_j)^2}{2\ln^2\sigma_j}\right) \tag{9}$$

where J is the number of modes, and D_j, σ_j, and w_j are the mean diameter, standard deviation, and the weight of the jth mode particle size distribution, respectively (Shao, 2001). Minimally and fully disturbed size distributions for different soil types were calculated using parameters for four soil textures, namely sand, loam, sandy clay loam, and clay, proposed by Shao (2004). Saltating particles can mobilize other particles with different size ranges by their impact on soil surface. Dust particles (defined as particulate matter < 70 μm) are not lifted by the direct effect of wind since the inter-particle cohesive forces are predominant compared to the aerodynamic forces (Kok et al., 2012). These particles are primarily ejected and lifted from the soil surface due to the impact of saltating particles on them (Gillette, 1974). This ejection from the soil results in a vertical dust particle flux into the atmosphere and subsequent particle suspension (which can be either short-term or long-term, depending on the size of the particles).

In this study, the following two methods were applied to estimate the vertical dust flux, F, from the dried lake bed:

1. A simplified total vertical dust flux F was obtained by modeling the ploughing process of individual saltating particles (assuming the impact angle of a saltating particle is 13°) as (Lu and Shao, 1999):

$$F = \frac{C_\alpha g f \rho_b}{2p}\left(0.24 + C_\beta u_* \sqrt{\frac{\rho_p}{p}}\right)Q \tag{10}$$

where p (500 for silty clay loam, 10,000 for loam, and 50,000 for sand dune) is the plastic pressure of the soil surface in Pa (surface

hardness), f is the fraction of dust contained in the volume of the soil, ρ_b and ρ_p are the densities of the bulk soil and particles, respectively, and C_α and C_β are constants; Q is the aggregate flux intensity determined by Eq. (6). For loamy and silty-clay loam which form 90% of the lake's saline playa, C_α is equal to 0.0002 and 0.0006, respectively; for sand dunes, C_α is 5. For C_β, the value of 1.37, suggested by Lu and Shao (1999), was applied for all soil textures. Here, f represents the fraction of mineral particles <10 μm and is equal to 15.2%, the average percentage of clay available in 12 samples gathered from the sites around the lake (Table 4).

2. A simplification of a vertical dust emission parameterization was followed in the second method (Shao, 2001). The proposed method for estimation of the vertical dust emission is based on saltation bombardment and aggregate disintegration mechanisms. Using this method, the dust emission rate for particle-size range with a mean value of d_i and an increment Δd_i, induced by saltation of particles of size d_s, can be calculated as:

$$F(d_i, d_s) = c_y \eta_{fi}[(1-\omega) + \omega\sigma_p](1+\sigma_m)\frac{gq(d_s)}{u_*^2} \quad (11)$$

where c_y is a dimensionless coefficient, $q(d_s)$ is the stream-wise saltation flux of particle with diameter d_s and g is the acceleration due to gravity. η_{fi} can be obtained by:

$$\eta_{fi} = \int_{d_i-\Delta d_i/2}^{d_i+\Delta d_i/2} p_f(d)\delta d \quad (12)$$

and σ_m is:

$$\sigma_m = 12u_*^2\frac{\rho_b}{p}\left(1+14u_*\sqrt{\frac{\rho_b}{p}}\right) \quad (13)$$

σ_p is the ratio of free dust to aggregated dust, i.e.:

$$\sigma_p = \frac{p_m(d_i)}{p_f(d_i)} \quad (14)$$

Assuming the particles are divided into I particle-size bins, each with a mean diameter d_i and an interval length Δd_i, the model proposed by Shao (2004) can be considered as a spectral dust emission model which can be utilized for estimation of the vertical dust flux of various particle size ranges. The vertical dust emission F from bin i is then:

$$F(d_i) = \int_{d_1}^{d_2} F(d_i, d)p(d)\delta d \quad (15)$$

where d_1 and d_2 are the lower and upper size limits for saltating particles. Total vertical dust emission of fine particulate matter is the sum of all size bins. The following values were assumed for p (required for calculation of σ_m) and c_y for different soil types (Shao, 2004): for sand dunes p = 1500 Pa and $c_y = 5\times10^{-5}$; for silty clay loam p = 50,000 Pa and $c_y = 1\times10^{-5}$; for loam p = 10,000 Pa and $c_y = 5\times10^{-5}$. To compute the density of air, the average air temperature of Urmia city of 21 °C was used, measured at the climate station between May and September, the driest period for the lake and a higher dust emission possibility. The average dew temperature between May and September for the Urmia climate station is 7.56 °C. Based on this, the average air density at the location of the lake of 10.32 kg m^{-3} was used. For the calculation of dynamic viscosity, it was assumed that the pressure is equal to the atmospheric pressure at sea level (since the change in air pressure has a minimal impact on the viscosity of gases). The dynamic viscosity of air was estimated at 18.17×10^{-6} Pa·s. Various parameterizations of vertical dust emission were compared with the wind tunnel (Roney and White, 2006) and in-field measurements (Nickling and Brown, 2001) of salty dust emission as a function of friction velocity to determine the best formulation for each soil texture (Fig. 5). In order to include the effects of moisture and non-erodible elements, the saltation threshold friction velocity should be corrected, usually by multiplication of the threshold friction velocity by correction factors >1. Soil moisture and the presence of non-erodible elements increase the saltation threshold friction velocity. Expanded parameterization of Fécan et al. (1998) was used for the correction of the soil moisture effect (Eq. SI.3). Moreover, the threshold friction velocity correction factor (f_λ) proposed by Raupach et al. (1993) was applied to account for the presence of roughness elements (Eq. SI.4).

3.4.3. Protecting farmers' income: Irrigation costs and subsidies

Currently, the irrigation efficiency in the Urmia basin is 41% (WRMC, 2007) and many endeavors are in progress to improve it to 70% or more for farms and 90% for horticultural gardens. However, in this study, a conservative assumption was made that the irrigation efficiency would increase only to 60%. Traditionally in Iran, the agricultural water price paid by farmers in modern, semi-modern, and traditional irrigation networks has been 1%, 2%, and 3% of the final value of the produced crop, respectively (WRMC, 2007). With this tariff scheme, farmers only pay 25% of the real calculated cost of water in three different irrigation networks and there is no incentive for improving the water use efficiency. In our optimization model, the irrigation water price of US$ 0.06 per m^3, recommended by the Iranian Ministry of Agriculture, was assumed to eliminate inefficiencies in the water consumption chain (WRMC, 2007). Alternatively, to protect farmers against a new irrigation water pricing system and capture climate-induced risks in crop yields, a new subsidy scheme was considered here. Prior to 2010, irrespective of the yield of harvested crops, farmers were entitled to receive fixed annual subventions. To be eligible for receiving the funding, it was assumed in this analysis that the farmers' harvested annual crop yield must fall below the 30th percentile of the historical local annual crop yields between 1995 and 2015 (based on data availability for all crop yields). With this subsidy scheme, we tried to cover the agriculture-associated risks throughout the growing season, including adverse climatic conditions, natural disasters, and pest invasions. The subsidy was estimated in US$ ha^{-1} as $Subsidy = a\times(yield)^b$, where yield is in t ha^{-1} and a and b are constant parameters for each cultivar. At lower yields, it was assumed that the payable subsidy increases with yield reduction compared to the reference yield. The final constant parameters used for each crop in the subsidy function based on historical yields are presented in Table 5. For some crops, including wheat, barely, and oil seeds, the final product price was calculated as a function of the yield to capture the high dependency of the final crop price on annual yields. In other words, the final crop price was assumed to be a function of the yearly crop yield because in years with low average crop yields, the final crop price increases.

3.4.4. Greenhouse gas emissions

The potential GHG emissions associated with the suggested land-use change were estimated at the optimal solution determined through the optimization model. The focus was on two major plausible activities: 1. conversion of the current marginal irrigated croplands to rain-fed systems; and 2. conversion of the current marginal croplands to grasslands/rangelands. Quantification of the change in GHG emissions as a result of shifting from one cropping pattern to another in irrigated lands is not as easy; hence, the change in GHG emissions related to the cropping pattern alteration within the irrigated croplands was not considered. For the conversion of irrigated to rain-fed croplands, we assumed that the current irrigated croplands in the river basins are converted into rain-fed cultivation of cereal crops. Furthermore, the conversion factors for the warm temperate dry IPCC climate zone were used to evaluate the change in the GHG emission in the

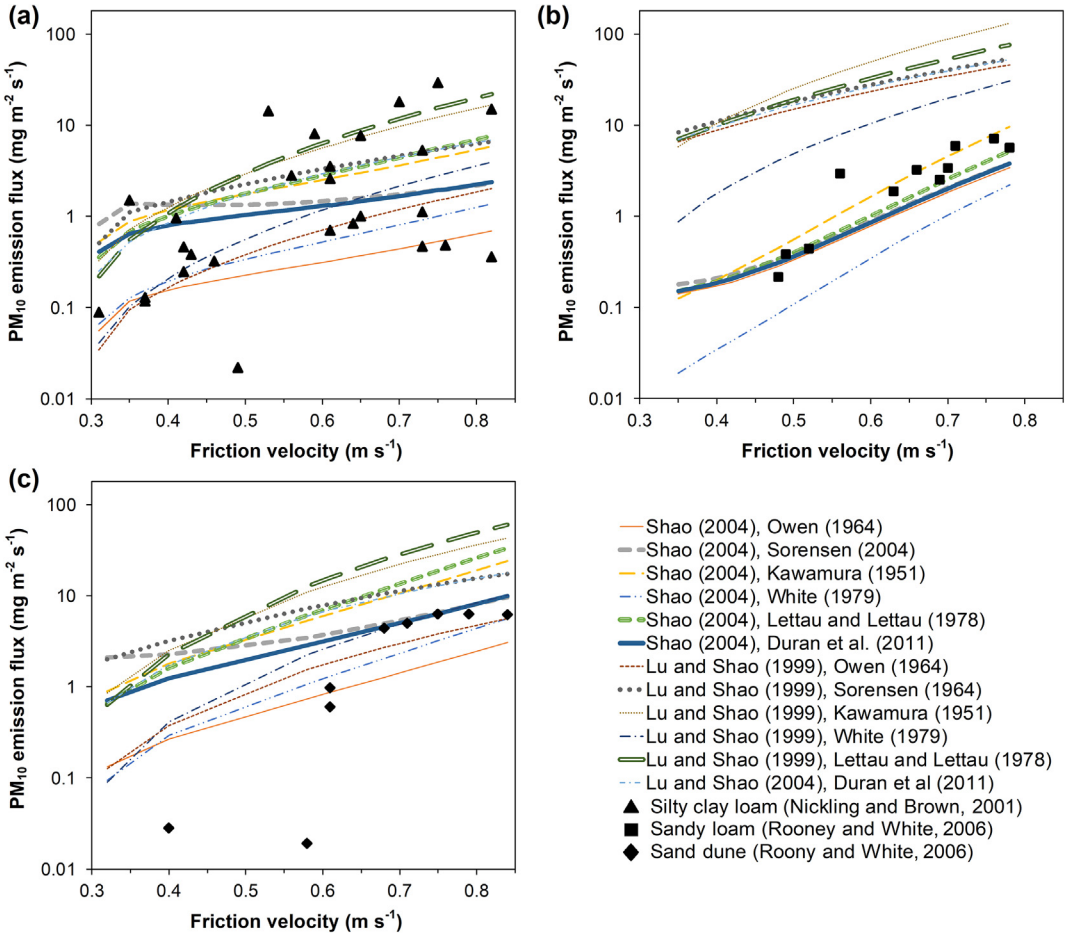

Fig. 5. Observed and modelled vertical PM_{10} emission from the Lake Urmia's saline playa: a. silty clay soil, b. sandy loam, and c. sand dune. Since there are no experimental data on saltation and vertical dust flux from the playa as a function of wind friction velocity, measured data for other saline lakes were used to assess and validate the performance of various vertical dust formulations. For each soil texture, measured values are shown as dots while model outputs are represented by the lines. For silty clay loam, the vertical PM_{10} dust emission rates were observed in an in-field wind-tunnel at potentially high emission areas in Owens Lake (Nickling and Brown, 2001). Experimental data for sandy loam and sand dunes were measured in the saltation wind-tunnel at University of California Davis (Roney and White, 2006) where crustal sediments were conveyed from Owens Lake to the wind-tunnel site. For silty clay loam, the horizontal saltation flux from White (1979) and vertical dust formulation from Lu and Shao (1999) were selected to model dust emissions from the Lake Urmia's bed. For sand dunes and sandy loam, White (1979) & Shao (2004) and Kawamura (1951) & Shao (2004) formulations were used, respectively.

Table 5
Historical annual yields, production costs, and average producer prices for different crops based on the data between 1995 and 2015.

Crop	Yield (30^{th} percentile) (t ha^{-1})	Production costs[a] (US$ ha^{-1})	Producer price[b] (US$ t^{-1})	*a*	*b*
Apple/pear	14.17	2547.82	605.59	2.14×10^{21}	−17.79
Stone fruits	9.54	6085.25	482.77	1.41×10^{18}	−19.75
Pistachio	0.63	7473.92	10042.24	0.01873	−7.14
Winter wheat	2.90	892.44	−0.0768 (yield) + 473.9	9.72×10^{6}	−13.15
Barely	2.64	680.51	−97.44 (yield) + 482.2	2.36×10^{15}	−39.23
Potato	22.14	2725.56	284.67	4.28×10^{43}	−33.46
Sugar beet	30.33	3025.31	95.10	8.85×10^{16}	−10.07
Oil seeds	0.97	1201.65	−274.7 (yield) + 871.9	0.03969	−12.84
Tomato	27.21	2783.12	237.80	1.10×10^{46}	−33.17
Cucumber	13.52	1331.60	422.95	1.76×10^{45}	−40.67
Water melons	9.85	1331.60	158.36	4.64×10^{45}	−48.59
Maize	5.92	1878.25	371.60	3.30×10^{18}	−24.21
Bean (dry)	1.14	1096.85	1616.97	2.15	−11.45

[a] Source: The Iranian Ministry of Agriculture for year 2014.
[b] Producer prices are adopted from FAO (2016) and show the final price received by farmers. For winter wheat, barely, and oil seed the producer prices are presented as function of the yield to capture the dependency of the price to produced crop availability. *a* and *b* are the constant parameters in the subsidy function.

Urmia basin. The sequestration rate was calculated by subtracting the average net soil CO_2 eq. emissions from the whole soil profile (0–1.2 m depth), with the clay contents of 18%, 34%, and 40% in the Australian cereal belt (Dalal and Chan, 2001), from the net cropland soil CO_2 eq. emissions of the IT-BCi site ($5,200 \pm 410$ kg CO_2 eq. ha^{-1} yr^{-1}), reported by Schaufler et al. (2010). We used these empirical values since the estimated emission rates of their studied site's IPCC climate zone are similar to the

Urmia basin's IPCC climate zone. For the restoration of cropland to grassland, we used the estimated emission factor range for the warm temperate dry IPCC climate zone (2,475–18,069 kg CO_2 eq. ha^{-1} yr^{-1}) in Diaz et al. (2012) to calculate the mean and standard deviation of the possible reduction in GHG emissions.

Conversion activities were studied in the context of two land-use change rates: achieving the land-use program targets in ten and in 30 years (Cameron et al., 2017). Monte Carlo simulation was used to propagate the uncertainty of the estimated emission rates for each land-based activity, with 50,000 iterations assuming normal distribution from the mean and standard deviation of the activity's net sequestration rate. The final probability distribution of each activity is the product of the Monte Carlo sampling results and the converted area rate. The 5th and 95th percentile of the cumulative reduction in GHG emissions of each activity during the conversion interval (ten or 30 years) were used to determine the confidence intervals.

4. Results and discussion

The following sections discuss the results obtained in the different steps of the framework.

4.1. Step 1: projected climate in the Urmia basin

Fig. 6 presents the overall variations in the projected changes in precipitation and near-surface (2 m) air temperatures (hereinafter referred to 'air temperature') across the Urmia basin, averaged by month. The results were computed by comparing air temperatures and precipitation outputs of each model for the reference (1960–1995) and future (2020–2050) periods. We chose 1960–1995 as the reference period because in that period the lake was in good condition and had high water levels. As can be inferred from Fig. 6, almost all the GCM ensemble members predict an increase in monthly air temperatures in the Urmia basin compared to the reference period. An increase in the basin's average monthly air temperatures was found for both 2050 scenarios: 1.95 °C for RCP 4.5 and 2.47 °C for RCP 8.5. A slightly lower increase is expected for the average annual temperature: 1.86 °C and 1.94 °C. Furthermore, a clear decreasing precipitation trend is projected to continue until 2050. The annual average precipitation in the basin is expected to decrease by 2.7% (RCP 4.5) and 11.6% (RCP 8.5) by 2050, relative to the reference period (1960–1995). The projected monthly precipitations show large seasonal variations. For RCP 4.5, the monthly precipitation ranges between −17.1% in August to 6.5% in December, while for RCP 8.5, all monthly precipitation are decreasing by up to −33.1% (September). In general, the decrease in precipitation rates is higher in spring and summer. However, it should be noted that the uncertainty analysis in Fig. 6 indicates a spectrum of possibilities with respect to precipitation, including no change, increase, and a greater reduction than discussed above.

In addition to the temperature and precipitation trends, a 52%-57% increase in the basin's population is anticipated by 2050 relative to the year 2007 (WRMC, 2007), further exacerbating the desiccation conditions if left unaddressed.

4.2. Step 2: salt water balance - the water required for restoration

As discussed in section 3.2, the results of the lake's salt balance in the period of shrinkage (1996–2010) suggest a considerable raise in the lake's floor due to the salt precipitation on the lake bed at a rate of 4 cm yr^{-1} (Fig. 7). Therefore, it can be concluded that the net inflow into the lake during the shrinkage was even

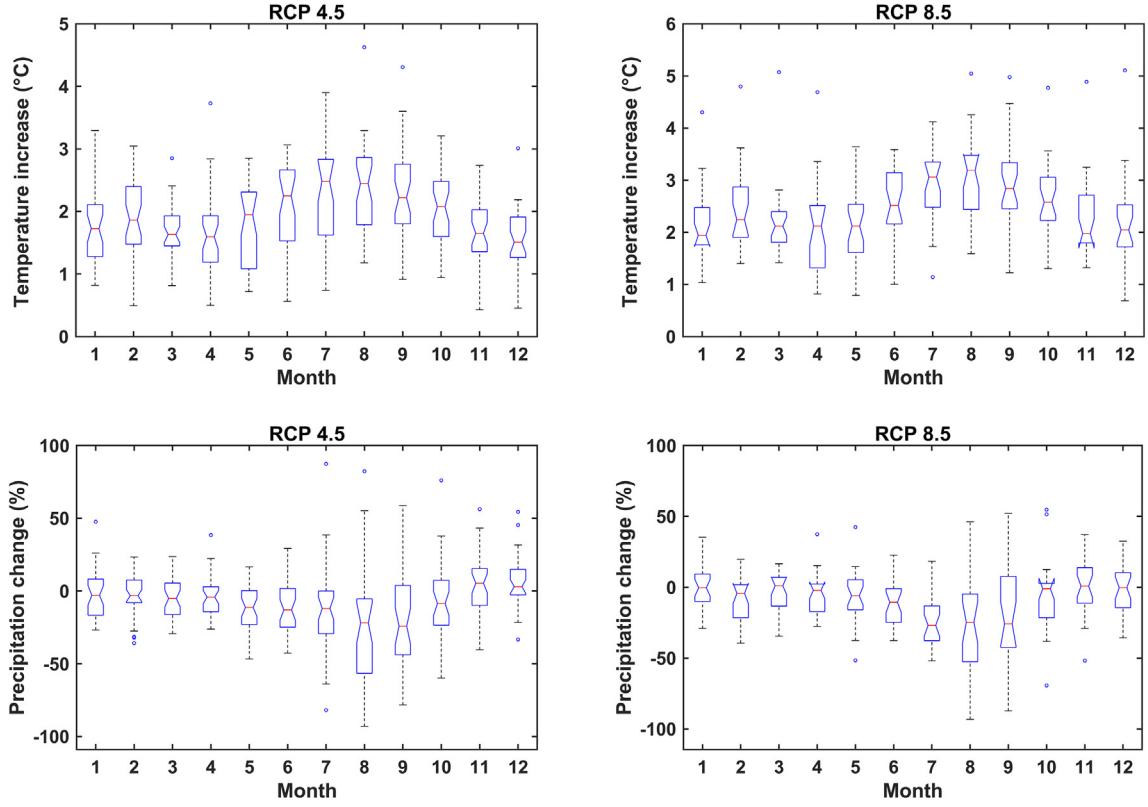

Fig. 6. Overall monthly variations in the projected changes in precipitation and near-surface air temperatures across the Urmia basin, calculated by comparing the output of each GCM ensemble member for the reference (1960–1995) and future (2020–2050) period. The central mark in each box indicates the median, and the bottom and top edges of the box are the 25th and 75th percentiles, respectively. The outliers are shown as individual dots.

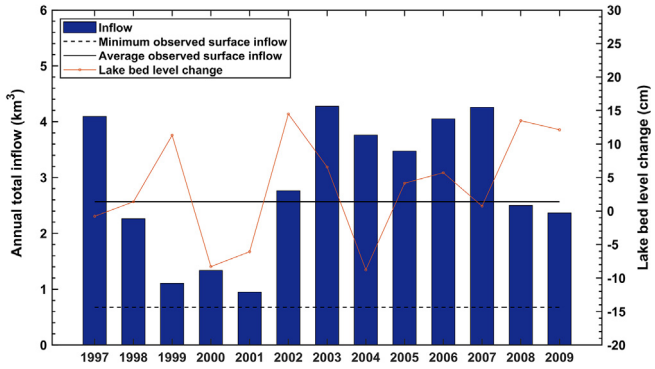

Fig. 7. Precipitated/dissolved salt on the lake bed and average annual total inflow into Lake Urmia, including both surface and underground flows (1997–2009). The average salt precipitation rate on the lake bed during the desiccation period is 0.04 m yr^{-1}.

smaller than the inflow value estimated here based only on the lake level-area-volume relationships. The precipitation of the salt on the lake bed is a result of the negative water balance and excess evaporation over the net inflow to the lake. As the lake's volume decreases, supersaturation of the dissolved salts causes precipitation of excessive salts on the lake bed.

It is generally accepted that Lake Urmia receives a comparatively small portion of its annual inflow from groundwater discharge. However, there is disagreement on the estimates of groundwater inflows, ranging from 3% (Hasemi, 2011) to 49% (JICA, 2016) of the total water input into the lake. The subsurface inflow to the lake is mainly through the wetlands around the lake because the thick halite bed does not allow for water flow through the lake bed (JICA, 2016). According to the results of our model, the average annual sub-surface inflow calculated as the difference between the total inflow (from the water balance analysis) and the surface water inflow (from stream gauges) varies only between 12.8% and 15.3%, depending on the method used for the estimation of annual evaporation. This indicates that the lake's water budget is mostly dependent on the surface inflow so that any future restoration plan should focus on increasing the amount of surface water flowing into the lake.

Fig. 8a shows the annual volume of surface water required for restoration of the lake by 2050 under the RCP 4.5 and RCP 8.5 scenarios for GCMs with the realization number of 1 (the other num-

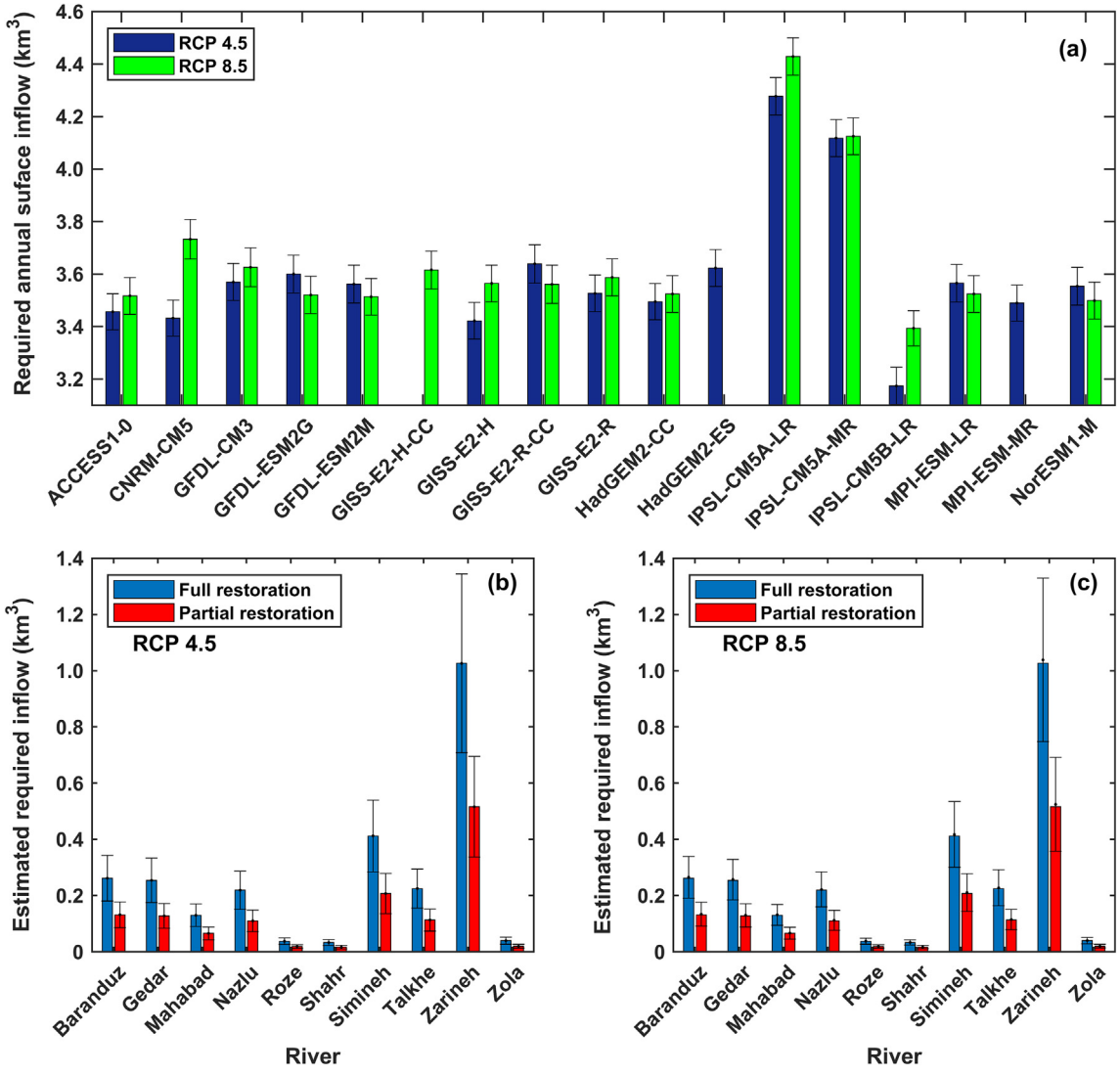

Fig. 8. a. Required annual surface inflow for restoration of the lake by 2050 under the RCP 4.5 and RCP 8.5 scenarios, predicted by the GCMs for the realization number of one. b and c. Minimum, maximum, and mean of the estimated annual volume of water required from each river supplying the lake (shown on the x-axis) for a ten-year partial (southern half of the lake) and 30-year full restoration of the lake.

bers are not shown for simplicity). These surface inflow requirements were estimated based on the bias-corrected evaporation and precipitation projected by the various GCMs. For each GCM, the uncertainty involved in the process of calibrating the hydrological balance over the lake's area was represented by the corresponding error bar (minimum and maximum required surface inflow values calculated by Monte Carlo simulations). According to the mass balance results, the average surface inflow of 3.648 $km^3\ yr^{-1}$ (standard deviation, SD = 0.271 km^3) is required under RCP 4.5 and 3.692 $km^3\ yr^{-1}$ (SD = 0.315 km^3) under RCP 8.5 for the complete 30-year lake restoration to the target level of 1274.1 m. Our predicted inflow is comparatively lower than that of JICA (2016) who estimated the annual river inflow volume of 4.95, 4.55, and 4.40 $km^3\ yr^{-1}$ for ten, 20, and 50 years' restoration scenarios, respectively. However, their model did not consider the projected climate variabilities to attain the target water level. Taking into account the annual sub-surface water gain of 12.8% in RCP 4.5 and 15.3% in RCP 8.5 (Fig. 7), our model shows that the total annual inflow required to restore the lake in 30 years is 4.183 $km^3\ yr^{-1}$ and 4.358 $km^3\ yr^{-1}$, respectively.

To put these results in perspective, the total current annual surface inflow to the lake is 2.13 $km^3\ yr^{-1}$. Therefore, under the RCP 4.5 scenario, a 70.8% increase in the inflow would be needed to rehabilitate the lake fully in 30 years' time; the equivalent increase for RCP 8.5 is 73.2%. As the sub-surface water gain is limited, much of the required water would need to be supplied by the lake's tributaries, with the water allocations shown in Fig. 8b and c (full restoration). This sensitivity to the surface inflow, as well as the substantial technical, institutional and behavioral barriers to reducing the upstream river withdrawals, make full restoration of the lake a grand challenge, particularly in the short term. Through a dynamic environmental inflow plan, Alborzi et al. (2018) predict that complete restoration of Lake Urmia under arid conditions may take up to 16 years even if a 40% decrease in the basin irrigation demand occurs. Therefore, partial restoration of the lake, similar to that implemented for the Aral Sea, could be a more promising approach to accelerate the rehabilitation process, as discussed next.

4.3. Steps 3 and 4: water allocation and optimal land use for agriculture

4.3.1. Short-term: recommended partial restoration

Decreased evaporation as a result of reduced surface area of the lake and the required water volume suggest that the current river inflows would be sufficient for a partial restoration of the lake. However, it is not clear which part of the lake should be prioritized for partial restoration based on the current river inflows. Some options have been proposed previously for partial restoration, including: 1. conserving the southern shores by building a dike connecting four major islands in the southern part of the lake (Razia et al., 2016) (hatched area in Fig. 9); and 2. dividing the lake into the northern and southern parts (Hamidi-Razi et al., 2018) (a two-lane highway embankment) and rehabilitating the southern part at the expense of the northern part. In addition to these, we also analyzed direct transfer of water to the northern part as a third option.

Since the wind dispersion of mineral aerosols from the dried bed lake is of major concern for environmental and human health (Gillette et al., 1997), here we prioritized the partial restoration option with the best potential for dust emission mitigation over other objectives, such as water quality, migratory birds, island separation, recreation, social, economic, and political, that can be fully, partially, or not at all achieved in partial restoration. To that end, we explored the main sources of PM_{10} through an intensity-frequency index analysis of remotely sensed AOT between 2010 and 2016 (the period with the highest shoreline recession). As a result, nine highly wind-erodible salt playa sites were detected, with an approximate aggregate area of 1,745.9 km^2 (Fig. 9).

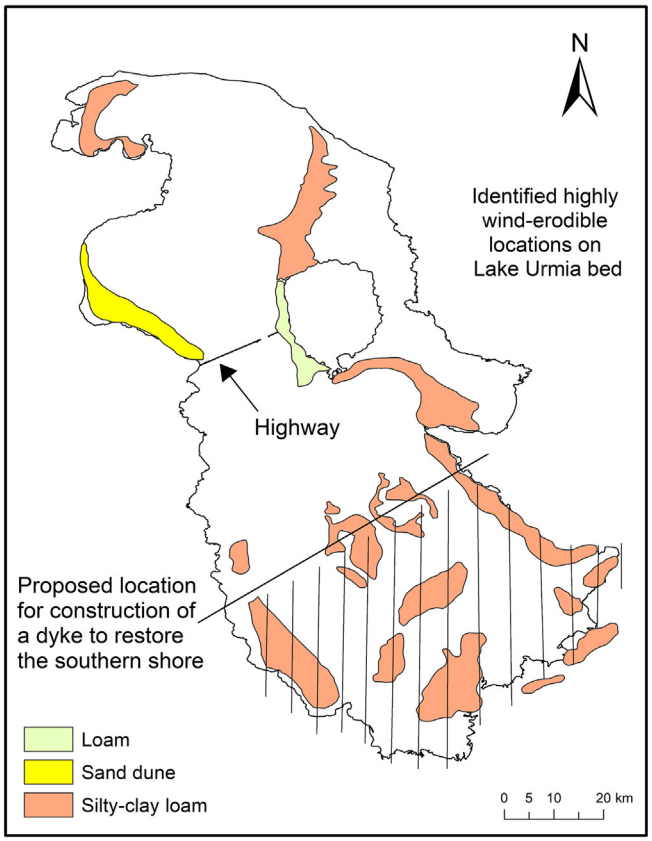

Fig. 9. Detected dust sources (coloured areas), their soil texture, and the proposed area for partial restoration. White areas represent the regions where no dust emissions are expected. The hatched area denotes the proposed area for restoration of four major islands.

Parametrizations of the vertical dust models were employed (see Section 3.4.2) to evaluate the potential for wind erosion from the lake bed as a function of soil moisture, vegetation cover, and texture. For the whole lake bed, meteorological records and vertical dust flux estimates show the potential for the release of 36,391 t $PM_{10}\ yr^{-1}$ contingent on the moisture of the bordering salty playa falling below the threshold moisture content for dust emissions (~5%). Based on our simulations, soil stabilization management, including ploughing, grooving, and planting salinity-tolerant seedlings to restore at least 5% of vegetative cover, were found to mitigate only 24.6% of the fugitive dust emissions. However, in the alternative scenario that keeps the soil moisture of the identified dust sources at 15%, the PM_{10} emissions would be reduced by 90.8%, to 3,342 t yr^{-1}. The likelihood of salt-entrained dust suspension can be reduced to almost zero by keeping the sediments moisture in the range of 35% to 40%.

Restoration of the southern half of the lake could mitigate 77% of salt-rich dust emissions from the lake bed. Restoration of the northern part of the highway (see Fig. 9) and areas below the main southern islands (hatched area in Fig. 9) could prevent 22% and 39% of the total average dust emissions per year, respectively. Thus, based on these results, restoration of the southern part of the lake should be given a higher priority. Diking would change the bathymetry, connectivity, and physics of the diked area, as well as the water and salt balances, and water level where the salinity tolerance is reached. Still, there is a challenge of defining a singular salinity and water level within the diked area. However, in case the ecological target

level for the whole lake (1,274.1 m) is attained in this southern part of the lake, the re-flooded areas would cover more than 70% of the detected dust-source locations of the whole lake. The Aji river in the northern part is responsible for 68% of the lake's annual dissolved salt entry (Table 2); therefore, the southern part receives a lower salt input. The decrease in salt concentration would allow for a recovery of the industry of harvesting brine-shrimp dormant eggs (or "cyst"). Under the RCP 4.5 and RCP 8.5 scenarios, our simulation shows that the respective annual water inputs of 1.83 and 1.86 km^3 can restore the southern part of the lake to the target level in ten years (Fig. 8b and c, partial restoration). Note that 1.58 km^3 of water is provided currently by the southern tributaries. The remaining volume of 0.32 km^3 can be supplied by the proposed land-use management, as discussed below.

4.3.2. Long-term restoration: recommended land-use change

In the short-term, partial restoration can help to redress the saline dust dispersion issue; however, the question about a sustainable solution for restoration of the lake still remains unanswered. Irrigation accounts for 93% of water consumption in the lake's basin, with an average irrigation efficiency of 37% for arable and 45% for horticultural lands (WRMC, 2007). One pragmatic and viable intervention to reduce the withdrawals would be to improve the irrigation efficiency or cultivation of less water-intensive crops (Micklin, 2007). It is unclear, however, how the current land use and crop distribution should be changed to use water more efficiently and achieve the required lake restoration target by 2050.

Using the optimization approach described in section 3.4, we determined the optimal land use and cropping patterns that maximize the farmers' net income at the river-basin level, subject to land and water availability. We divided the irrigated area in the Urmia basin into six major zones, represented in Fig. 10, with the suggested decrease in irrigated areas and change in cropping patterns in these sub-basins given in Fig. 11. These results are based on the analysis of the effects of regional climate change (for RCP 4.5 and RCP 8.5), expansion of upstream irrigation reservoirs/networks, and population growth along the major tributaries of the lake, considering two plausible lake restoration options: intra-basin restoration (without any human-made water conveyance) and inter/*trans*-basin restoration (partly relying on water diversion from the Zab basin).

In the case of intra-basin restoration, our results show that optimal water use over the basin requires the conversion of 95,600 ha (RCP 4.5) and 133,687 ha (RCP 8.5) of irrigated land for rain-fed cropland or grassland. Under RCP 4.5, the optimal reduction in horticultural lands (31%) is slightly higher than in the arable lands (28%). Likewise, under RCP 8.5, the optimal reduction in horticultural lands is 34% and in arable 30%. The annual water requirement for restoration of the lake by 2050 are 3,648 and 3,692 $Mm^3\ yr^{-1}$ for RCP 4.5 and RCP 8.5, respectively.

For inter-basin restoration, a reduction of 78,700 ha and 114,826 ha in the total irrigated area is proposed under the RCP 4.5 and 8.5 scenarios. This is significantly reduced compared to the area currently used for cultivation in the lake's basin, which

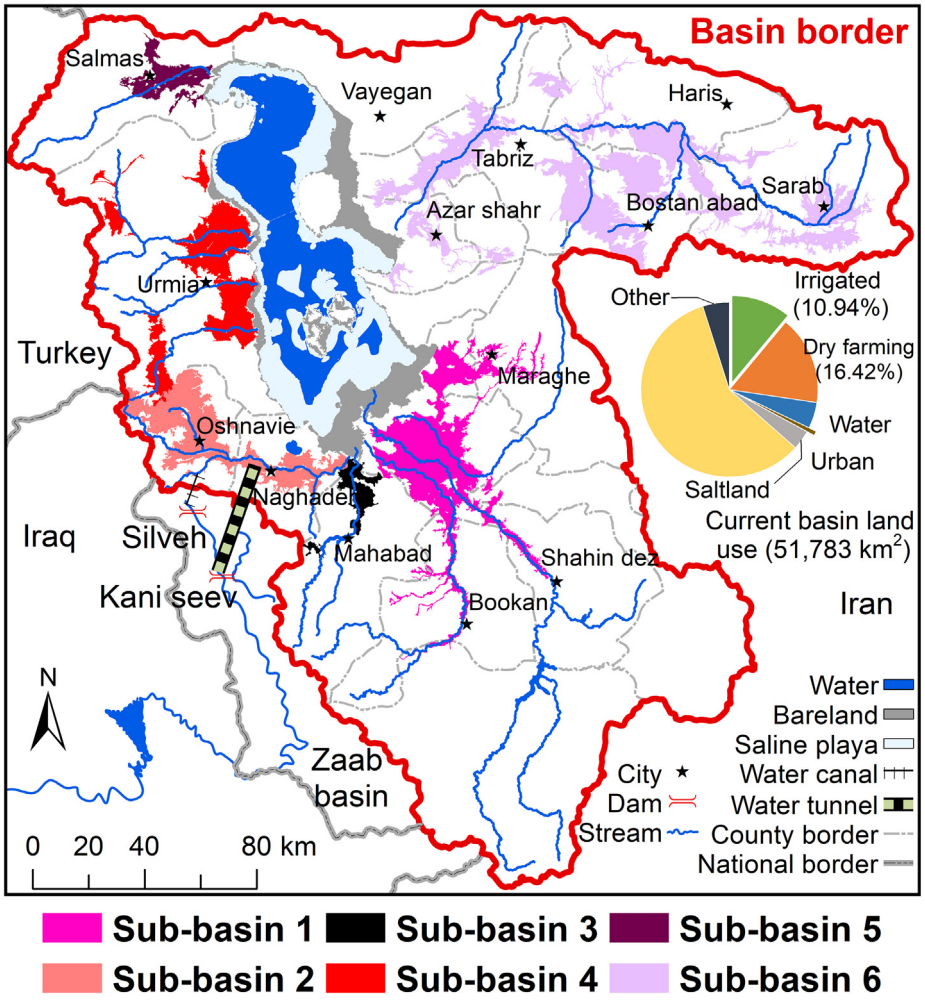

Fig. 10. The Urmia basin and six major agricultural sub-basins considered in the study.

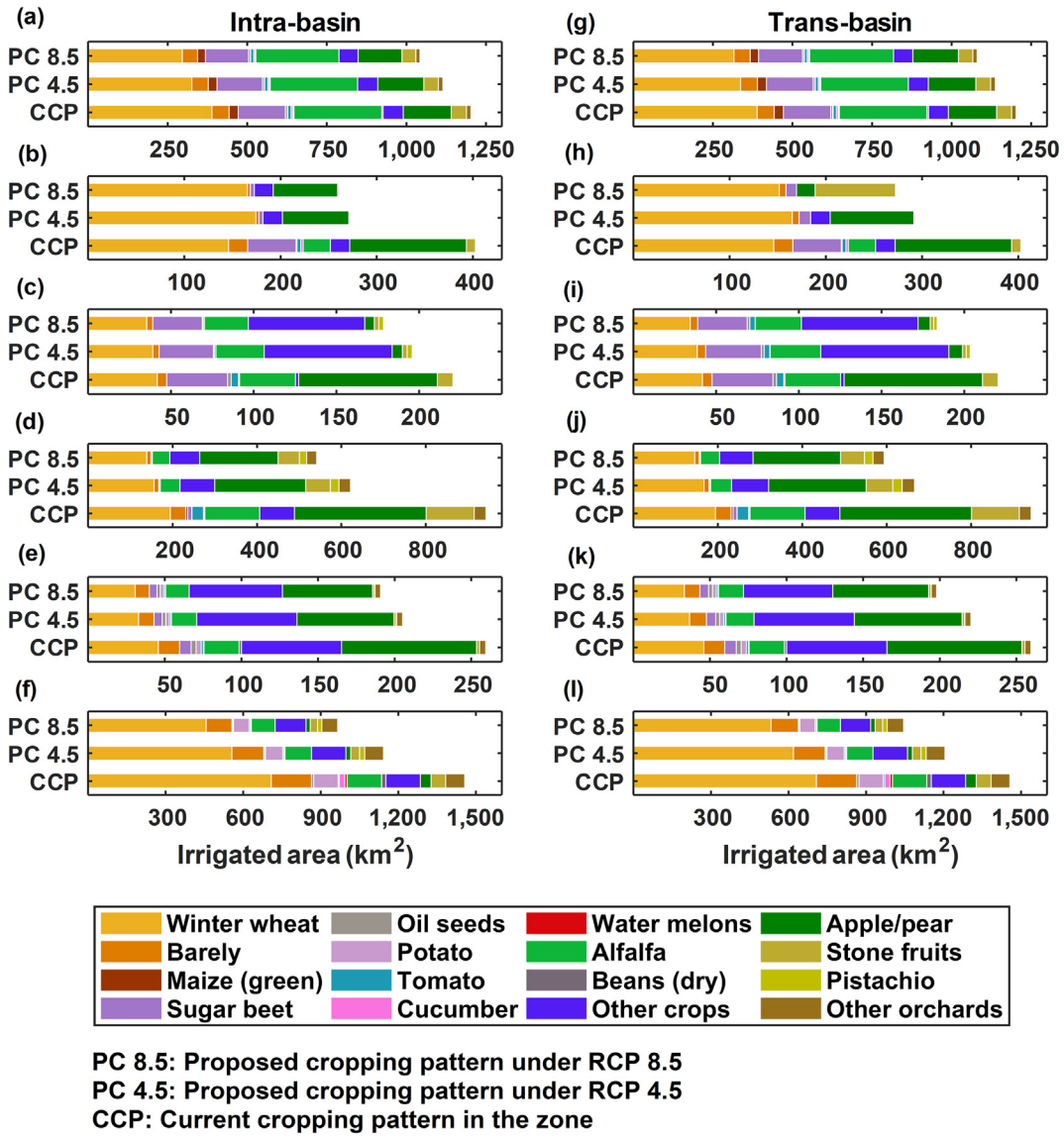

Fig. 11. Proposed land-use change in the Lake Urmia's basin for the restoration of the lake by 2050. Each bar chart shows the proposed change in the current area under cultivation in the agricultural sub-basins (shown in Fig. 10) considering 14 major crop categories. New cropping patterns refer to two options: intra-basin restoration of the lake (a to f) and inter-basin restoration (g to l). Consideration was given to the role of the major stressors: rise in the basin's temperature, increase in population/dry years, and completion of upstream reservoirs and irrigation networks.

is close to 438,900 ha (Fig. 12). The total inflow into the lake required for this restoration option is 3,048 and 3,092 $Mm^3\ yr^{-1}$ for the two respective scenarios.

For the optimal cropping pattern in the basin in both restoration options, ~624 mm (RCP 4.5) and ~681 mm (RCP 8.5) of water per year would satisfy the irrigation demand of the basin (at 60% irrigation efficiency); by comparison, 1,511 mm is used currently (WRMC, 2007).

At the end of the 30-year restoration process, assuming the current final price for the crops considered, we estimated under RCP 4.5 that the unit water productivity would be 0.278 US$ m^{-3} for the inter-basin water transfer and 0.304 US$ m^{-3} for the intra-basin restoration. This represents a respective increase of 68% and 87% from the current water productivity of 0.16 US$ m^{-3}. Similar increases were found for the two restoration options under RCP 8.5: 0.271 US$ m^{-3} and ~0.296 US$ m^{-3}, respectively.

Regarding the change in cropping patterns, the share of each crop group would remain generally the same as currently (Fig. 12). However, the share of individual crops would change, favouring crops, which require less water (Fig. 11). One such crop is pistachio so its proposed cultivation would increase in intra-basin restoration from the current 718 ha to 4,415 ha (RCP 4.5) and 3,790 ha (RCP 8.5), mostly in areas downstream of the river basins. For inter-basin restoration, the pistachio cultivation would increase to 4,542 ha (RCP 4.5) and 4,038 ha (RCP 8.5). This would also lead to a large increase in farmers' revenue as pistachio has a high final (market) price.

According to the crop yields and the area under cultivation in each year until 2050, our calculations showed that the final annual subsidy cost to cover the new irrigation water cost would be US$ 1.179 million (RCP 4.5) and US$ 1.287 million (RCP 8.5) for intra-basin restoration. For the inter-basin option, these values decrease to US$ 0.995 million (RCP 4.5) and US$ 1.105 million (RCP 8.5), respectively. Overall, winter wheat, barley, and maize need the highest average annual subsidy (9.17, 1.25, and 4.64 US$ ha^{-1}).

The proposed change in land use and cropping patterns would lead to a reduction in GHG emissions (Table 6). This is due to the reduction in the area of land used for cultivation of 21% (RCP 4.5)

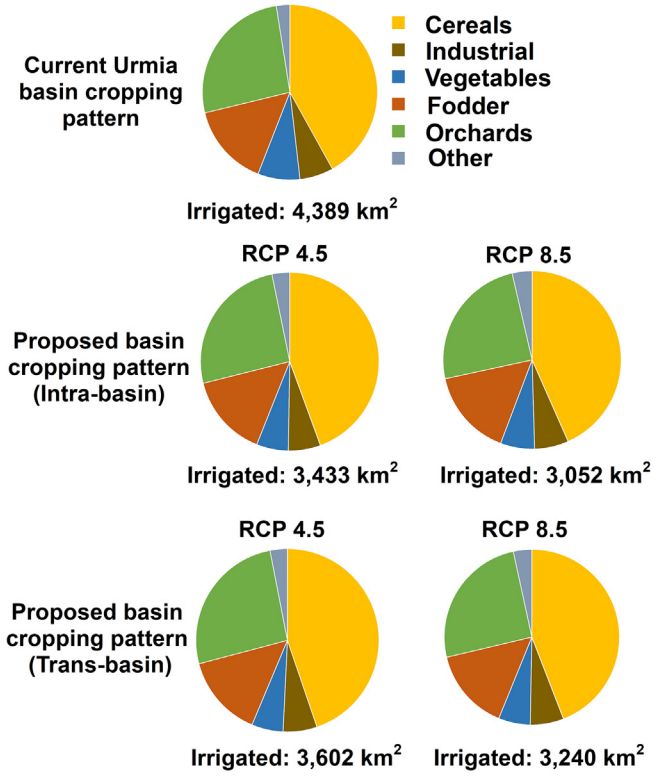

Fig. 12. Proposed cropping pattern change in the Urmia basin (Cereals: wheat, barely, maize; industrial crops: sugar beet, oil seeds; vegetables: potato, tomato, cucumber, water melons, bean, sweet melon, onion, and other vegetables; fodder: clover, alfalfa, corn; orchards: apples, grapes, stone fruits, pistachio, and others).

to 30% (RCP 8.5) for the intra-basin restoration option. As indicated in Table 6, conversion of the irrigated croplands to rain-fed crops and to grasslands would reduce the cumulative GHG emission from 0.07 (0.05–0.09) Mt CO_2 eq. to 1.55 (0.65–2.44) Mt CO_2 eq., depending on the type, amount, and speed of conversion. On average, changing from irrigated croplands to grasslands saves six times more GHG emissions than converting to rain-fed cropland. As expected, the mitigated GHG emissions are higher over the ten-year restoration period than over 30 years.

It should be noted that the GHG savings refer only to land-use change (section 3.4.4) and do not include GHG emissions as a result of farming activities. It is also noteworthy that there is a general lack of data on GHG emissions related to alteration of cropping patterns within the irrigated croplands for a region with climatic parameters similar to the Urmia basin. For example, there are no data for the change in GHG emissions due to a change from wheat to sugar beet cultivation. Therefore, with the available data it was not possible to include GHG emissions in the optimization model and hence the GHG emissions have been estimated at the optimum solution. However, in other saline lakes' basins where detailed data on GHG emissions related to changing a crop pattern are available, the emissions can be included into the optimization model.

The aforementioned reductions in the total area under cultivation, especially, without water transfer from adjacent basins, would entail some behavioral and institutional challenges that can jeopardize the accomplishment of the land-use strategies proposed in this study. This is particularly the case in the Urmia, Gedar, and Aji sub-basins due to the required large-scale land-use reduction in the agricultural sector (up to 42%, 35%, and 33%, respectively). Indeed, these strategies go against the current tendency to increase crop production at the farm level and therefore their implementation may meet major opposition. Monetizing the activities involved in conversion of the irrigated lands to grasslands/rangelands or rain-fed systems is difficult with available data; however, investing in entrepreneurial initiatives to reduce the local livelihood dependency on agriculture and industrializing the economy of the Urmia basin would presumably ensure long-term profits.

4.4. Method limitations and uncertainties

In addition to the uncertainties in future climate projections, there are some other limitation to the methodologies used in the proposed framework. For instance, there may be some bias in the historical climatic data used as observations to remove the significant bias in the output of GCMs. Use of the data from meteorological stations, combined with more advanced bias-correction methods (e.g. quantile-mapping (Gudmundsson et al., 2016)) may mitigate this issue.

Another limitation is the reference period for calibration of the hydrological balance over the lake's area. Here, the period from 1995 to 2010 was considered with yearly time resolutions, while longer periods with finer time resolutions (e.g. monthly) would improve the accuracy of the results.

One of the sources of uncertainty in the estimations of the dust release from Lake Urmia bed is the data that we used for validation of the vertical dust parametrizations, which are not specific to this lake. Long-term experimental data on the response of the lake's playa to wind erosion are rare and require further laboratory and field studies. Similarly, most of the data that we used as crop tuning parameters were the general crop parameters adopted from Allen et al. (2005). More detailed data from the cultivars in the Urmia basin would improve the simulations of the crop-yield response.

Furthermore, the restored lake and its surrounding wetlands can act as carbon sinks. With the available data, quantifying their potential for carbon sequestration was not possible and was not considered in the study. This could be a subject of future work.

Table 6
Reductions in GHG emissions as a result of the proposed land use change in the agricultural sector over ten- and 30-year periods.

Restoration option	Scenario	Period	Cropland to rain-fed (Mt CO_2 eq.)			Cropland to grassland (Mt CO_2 eq.)		
			5th percentile[a]	Median	95th percentile[a]	5th percentile[a]	Median	95th percentile[a]
Intra-basin	RCP 4.5	10 years	0.18	0.27	0.36	0.46	1.02	1.60
		30 years	0.06	0.09	0.12	0.47	1.11	1.74
	RCP 8.5	10 years	0.38	0.38	0.50	0.64	1.40	2.37
		30 years	0.08	0.12	0.16	0.65	1.55	2.44
Inter-basin	RCP 4.5	10 years	0.15	0.22	0.29	0.37	0.88	1.39
		30 years	0.05	0.07	0.09	0.39	0.90	1.43
	RCP8.5	10 years	0.22	0.33	0.43	0.55	1.29	2.02
		30 years	0.07	0.10	0.14	0.65	1.54	2.43

[a] Calculated through Monte Carlo simulation.

5. Conclusions

A new eco-hydrological framework was proposed to pave the way for preservation and restoration of desiccating saline lakes in the face of projected climate change, with the aim of mitigating the catastrophic consequences of their shrinkage. The framework comprises a suit of models used to identify optimal solutions for lake restoration, including global circulation, salt-water, water allocation, and land-use and economic optimization models. Considering the effects of global warming under different climate change scenarios, the framework enables estimations of the amount of water required for either partial or full restoration of saline lakes based on the water availability in the lake's tributaries. It also guides decision and policy makers in formulating an optimal land-use strategy in the lake's basin with the aim of restoring the lake to recommended ecological levels up to 2050.

To illustrate its capabilities, the framework was applied in the context of a typical saline lake's basin, in this case Lake Urmia. This lake used to be the second hyper-saline lake in the world and has faced a drastic water-level decline over the past two decades. The following conclusions can be drawn with respect to the restoration of Lake Urmia, based on the application of the proposed framework:

- The outputs of the GCMs suggest an increase of ~2 °C in the average temperature in the basin by 2050 compared to the reference period (1960–1995). A decreasing precipitation trend is expected by 2050, although the uncertainty analysis suggest a spectrum of possibilities, from no change, to an increase to a greater decline in precipitation.
- The mass and water balance model over the lake's area between 1997 and 2010 (shrinkage period) shows the salt precipitation of 4 cm yr^{-1} on the lake bed. The subsurface flow in this period was limited, ranging between 12.8% and 15.4% of the total inflow to the lake of 2,861.3 Mm^3 yr^{-1}.
- The average surface inflow of water required for a complete 30-year lake restoration to the target level of 1,274.1 m was estimated at 3,648 Mm^3 $yr^{-1}$for the RCP 4.5 scenario and 3,692 Mm^3 yr^{-1} for RCP 8.5. From a policy perspective, increase in population, maintaining equity among stakeholders, and various financial, behavioral and institutional barriers impede attaining such surface inflows in the short-term. Instead, partial restoration of the lake by 2030 might be a more feasible option.
- If the soil moisture of the lake bed falls below 5%, there is a potential for the release of 36,391 t yr^{-1} of saline PM_{10} from the lake bed. These emissions would reduce to 3,342 t yr^{-1} with the soil moisture increasing to 15%. Restoration of the southern half of the lake could mitigate 77% of salt-rich dust emissions from the lake bed, while restoration of the northern and areas below the main southern islands could prevent only 22% and 39% of the total average dust emissions per year, respectively. Accordingly, the restoration of the southern part of the lake is recommended in the short-term (2030) to control the expected PM_{10} emissions from the lake bed.
- An annual water input of 1.83 km^3 (RCP 4.5) and 1.86 km^3 (RCP 8.5) can restore the southern part of the lake to the target level of 1,274.1 m in ten years; currently, 1.58 km^3 of water is provided by the southern tributaries.
- At present, the area under cultivation in the lake's basin is close to 438,900 ha. In the case of restoration, including inter-basin water transfers, a reduction in the total irrigated area of 78,700 ha is proposed under RCP 4.5 and 114,826 under RCP 8.5. The conversion of 95,600 ha (RCP 4.5) and 133,687 ha (RCP 8.5) of irrigated lands to rain-fed cropland or grassland is suggested.
- At the end of the 30-year restoration plan, the unit water productivity would be 0.278 US$ m^{-3} for restoration with inter-basin water transfer and 0.304 US$ m^{-3} for the intra-basin restoration scenario (RCP 4.5). The equivalent values for RCP 8.5 are 0.271 US$ m^{-3} and 0.296 US$ m^{-3}, respectively.
- Conversion of the irrigated croplands to rain-fed systems and to grasslands proposed here is expected to reduce cumulative GHG emissions due to the land-use change from 0.07 (0.05–0.09) Mt CO_2 eq. to 1.55 (0.65–2.44) Mt CO_2 eq., depending on the type, amount, and speed of land conversion.

As demonstrated in the paper, the proposed framework provides a comprehensive and powerful tool to aid decision and policy makers in identifying optimal solutions for restoring saline lakes at risk of desiccation. The framework is generic enough to be applicable to different regions, subject to data availability. It is recommended that future work explores its application to other saline lakes with the aim of demonstrating further its applicability and improving the methods.

Conflict of interest

The authors declare no conflict of interest.

Acknowledgements

Nima Shokri acknowledges the funding by Royal Academy of Engineering-The Leverhulme Trust Senior Research Fellowship (LTSRF1718\14\8). We acknowledge the use of imagery from the NASA Worldview application (https://worldview.earthdata.nasa.gov/) operated by the NASA/Goddard Space Flight Center Earth Science Data and Information System (ESDIS) project. The authors would like to thank MIKE powered by the DHI group in Denmark for providing the Mike HYDRO basin management framework. The first author's PhD study is supported by Presidential Doctoral Scholarship Award at The University of Manchester which is gratefully acknowledged.

Appendix A. Supplementary data

Supplementary data to this article can be found online at https://doi.org/10.1016/j.scitotenv.2019.134718.

References

Abbaspour, M., Nazaridoust, A., 2007. Determination of environmental water requirements of Lake Urmia, Iran: an ecological approach. Int. J. Environ. Stud. 64, 161–169.
Abuduwaili, J., DongWei, L., GuangYang, W., 2010. Saline dust storms and their ecological impacts in arid regions. J. Arid Land 2, 144–150.
AghaKouchak, A., Norouzi, H., Madani, K., Mirchi, A., Azarderakhsh, M., Nazemi, A., et al., 2015. Aral Sea syndrome desiccates Lake Urmia: call for action. J. Great Lakes Res. 41, 307–311.
Alborzi, A., Mirchi, A., Moftakhari, H., Mallakpour, I., Alian, S., Nazemi, A., et al., 2018. Climate-informed environmental inflows to revive a drying lake facing meteorological and anthropogenic droughts. Environ. Res. Lett. 13, 084010.
Alipour, S., Mosavi-ovenlegi, K., Hosseini, E., Aslanpour, S., Haseli, Z., 2018. Geochemistry of major, trace and rare earth elements in bed-sediments of Urmia lake. J. Geosci. 27, 51–62.
Allen, R.G., Pereira, L.S., Smith, M., Raes, D., Wright, J.L., 2005. FAO-56 dual crop coefficient method for estimating evaporation from soil and application extensions. J. Irrig. Drain. Eng. 131, 2–13.
Altinbilek, D., 2004. Development and management of the Euphrates-Tigris basin. Int. J. Water Resour. Dev. 20, 15–33.
Cameron, D.R., Marvin, D.C., Remucal, J.M., Passero, M.C., 2017. Ecosystem management and land conservation can substantially contribute to California's climate mitigation goals. Proc. Natl. Acad. Sci. 114, 12833–12838.
Chaudhari, S., Felfelani, F., Shin, S., Pokhrel, Y., 2018. Climate and anthropogenic contributions to the desiccation of the second largest saline lake in the twentieth century. J. Hydrol. 560, 342–353.

Dalal, R., Chan, K., 2001. Soil organic matter in rainfed cropping systems of the Australian cereal belt. Soil Res. 39, 435–464.
Darvishi J., 2014. Lymphology and Paleolymology Report of Lake Urmia: the balance of water and salt and the sedimentation rate of salts, Final report (in Farsi). Geological Survey of Iran, Iran.
Deatrick, E., 2016. Can a controversial canal stop thousands of sinkholes from forming around the Dead Sea. Science 22.
Diaz, D., Rashford, B., De Gryze, S., Zakreski, S., Dell, R., 2012. Evaluation of avoided grassland conversion and cropland conversion to grassland as potential carbon offset project types. The Climate Trust, Portland, Oregon.
Draxler, R.R., 1999. HYSPLIT, radiological transport and dispersion model implementation on NCEP Cray: Silver Spring, Maryland : U.S. Department of Commerce, National Oceanic and Atmospheric Administration. National Weather Service, Office of Meteorology, Science Division.
Durán, O., Claudin, P., Andreotti, B., 2011. On aeolian transport: grain-scale interactions, dynamical mechanisms and scaling laws. Aeolian Res. 3, 243–270.
Emori, S., Taylor, K., Hewitson, B., Zermoglio, F., Juckes, M., Lautenschlager. M., et al., 2016. CMIP5 data provided at the IPCC Data Distribution Centre. Geneva.
FAO United Nations, 2016. Statistics database.
Fathian, F., Morid, S., Kahya, E., 2015. Identification of trends in hydrological and climatic variables in Urmia Lake basin, Iran. Theoret. Appl. Climatol. 119, 443–464.
Fécan, F., Marticorena, B., Bergametti, G., 1998. Parametrization of the increase of the aeolian erosion threshold wind friction velocity due to soil moisture for arid and semi-arid areas. Annales Geophysicae. 17. Springer, pp. 149–157.
García-Vila, M., Fereres, E., 2012. Combining the simulation crop model AquaCrop with an economic model for the optimization of irrigation management at farm level. Eur. J. Agron. 36, 21–31.
Garousi, V., Najafi, A., Samadi, A., Rasouli, K., Khanaliloo, B., 2013. Environmental crisis in Lake Urmia, Iran: a systematic review of causes, negative consequences and possible solutions. Proceedings of the 6th International Perspective on Water Resources & the Environment (IPWE) Izmir, Turkey.
Ghale, Y.A.G., Altunkaynak, A., Unal, A., 2018. Investigation anthropogenic impacts and climate factors on drying up of Urmia Lake using water budget and drought analysis. Water Resour. Manage. 32, 325–337.
Gillette, D.A., 1974. On the production of soil wind erosion aerosols having the potential for long range transport. J. Rech. Atmos 8, 735–744.
Gillette, D.A., Fryrear, D., Xiao, J.B., Stockton, P., Ono, D., Helm, P.J., et al., 1997. Large-scale variability of wind erosion mass flux rates at Owens Lake: 1. Vertical profiles of horizontal mass fluxes of wind-eroded particles with diameter greater than 50 μm. J. Geophys. Res. Atmos. 102, 25977–25987.
Gudmundsson, L., 2016. QMAP: Statistical transformations for post-processing climate model output. R package version 1.0-4, 1.0–3.
Hamidi-Razi, H., Mazaheri, M., Carvajalino-Fernández, M., Vali-Samani, J., 2018. Investigating the restoration of Lake Urmia using a numerical modelling approach. J. Great Lakes Res.
Hammer, U.T., 1986. Saline Lake Ecosystems of the World Vol 59.
Harris, I., Jones, P.D., Osborn, T.J., Lister, D.H., 2014. Updated high-resolution grids of monthly climatic observations–the CRU TS3 10 Dataset. Int. J. Climatol. 34, 623–642.
Hasemi, M., 2011. A socio-technical assessment framework for integrated water resources management (IWRM) in Lake Urmia Basin. Iran.
Hassanzadeh, E., Zarghami, M., Hassanzadeh, Y., 2012. Determining the main factors in declining the Urmia Lake level by using system dynamics modeling. Water Resour. Manage. 26, 129–145.
Hawkins, E., Osborne, T.M., Ho, C.K., Challinor, A.J., 2013. Calibration and bias correction of climate projections for crop modelling: an idealised case study over Europe. Agric. For. Meteorol. 170, 19–31.
Hengl, T., de Jesus, J.M., Heuvelink, G.B., Gonzalez, M.R., Kilibarda, M., Blagotić, A., et al., 2017. SoilGrids250m: Global gridded soil information based on machine learning. PLoS ONE 12, e0169748.
Hobbs, R.J., Norton, D.A., 1996. Towards a conceptual framework for restoration ecology. Restor. Ecol. 4, 93–110.
Houghton, R.A., 2003. Revised estimates of the annual net flux of carbon to the atmosphere from changes in land use and land management 1850–2000. Tellus B 55, 378–390.
Jalili, S., Hamidi, S.A., Namdar, Ghanbari R., 2016. Climate variability and anthropogenic effects on Lake Urmia water level fluctuations, northwestern Iran. Hydrol. Sci. J. 61, 1759–1769.
JICA, 2016. Data collection survey on hydrological cycle of lake Urmia basin in the Islamic Republic of Iran.
Kang, J.Y., Yoon, S.C., Shao, Y., Kim, S.W., 2011. Comparison of vertical dust flux by implementing three dust emission schemes in WRF/Chem. J. Geophys. Res. Atmos., 116
Kawamura, R., 1951. Study of sand movement by wind Translated, (1965) as University of California Hydraulics Engineering Laboratory Report HEL 2-8, Berkely.
Kelts, K., Shahrabi, M., 1986. Holocene sedimentology of hypersaline Lake Urmia, northwestern Iran. Palaeogeogr. Palaeoclimatol. Palaeoecol. 54, 105–130.
Kok, J.F., Parteli, E.J., Michaels, T.I., Karam, D.B., 2012. The physics of wind-blown sand and dust. Rep. Prog. Phys. 75, 106901.
Kottek, M., Grieser, J., Beck, C., Rudolf, B., Rubel, F., 2006. World map of the Köppen-Geiger climate classification updated. Meteorol. Z. 15, 259–263.
Lensky, N., Dvorkin, Y., Lyakhovsky, V., Gertman, I., Gavrieli, I., 2005. Water, salt, and energy balances of the Dead Sea. Water Resour. Res. 41.
Lettau, K., Lettau, H., 1978. Experimental and micrometeorological field studies of dune migration. In: Lettau, H.H., Lettau, K., (Eds.) Exploring the world's driest climate. Madison.
Levy, R., Hsu, C., 2015. Modis atmosphere l2 aerosol product, NASA modis adaptive processing system, Goddard Space Flight Center, USA.
Lu, H., Shao, Y., 1999. A new model for dust emission by saltation bombardment. J. Geophys. Res. Atmos. 104, 16827–16842.
Madani, K., 2014. Water management in Iran: what is causing the looming crisis? J. Environ. Stud. Sci. 4, 315–328.
Mathworks T. Matlab Optimization Toolbox User's Guide.
McCune, D., 1991. Effects of airborne saline particles on vegetation in relation to variables of exposure and other factors. Environ. Pollut. 74, 176–203.
Messager, M.L., Lehner, B., Grill, G., Nedeva, I., Schmitt, O., 2016. Estimating the volume and age of water stored in global lakes using a geo-statistical approach. Nat. Commun. 7, 13603.
Micklin, P., 2007. The Aral sea disaster. Annu. Rev. Earth Planet. Sci. 35, 47–72.
Mike, 2017. Hydro Basin User Guide.
Miller, J.R., 1987. The Political Economy of Western Water Finance: Cost Allocation and the Bonneville Unit of the Central Utah Project. Am. J. Agric. Econ. 69, 303–310.
Mohammed, I.N., Tarboton, D.G., 2012. An examination of the sensitivity of the Great Salt Lake to changes in inputs. Water Resour. Res. 48.
Mor, Z., Assouline, S., Tanny, J., Lensky, I., Lensky, N., 2018. Effect of water surface salinity on evaporation: The case of a diluted buoyant plume over the Dead Sea. Water Resour. Res. 54, 1460–1475.
Nickling, W.G., Brown, L.J., 2001. PM10 Dust Emissions At Owen Lake, CA 2001, Final Report.
Owen, P.R., 1964. Saltation of uniform grains in air. J. Fluid Mech. 20, 225–242.
Pekel, J.F., Cottam, A., Gorelick, N., Belward, A.S., 2016. High-resolution mapping of global surface water and its long-term changes. Nature 540, 418.
Raes, D., Steduto, P., Hsiao, T.C., Fereres, E., 2009. AquaCrop—the FAO crop model to simulate yield response to water: II. Main algorithms and software description. Agron. J. 101, 438–447.
Rahi, K.A., Halihan, T., 2018. Salinity evolution of the Tigris River. Reg. Environ. Change 18, 2117–2127.
Raupach, M., Gillette, D., Leys, J., 1993. The effect of roughness elements on wind erosion threshold. J. Geophys. Res. Atmos. 98, 3023–3029.
Razia, H.H., Mazaherib, M., Samanic, J.M.V., Fernandezd, M.C., 2016 Investigating Urmia Lake Partial Restoration and Ecological Water Level Using MOHID-2D Water Hydrodynamic Model. Geographic and Environmental Impacts of Urmia Lake Conditions Conference, Tabriz, Iran.
Rolph, G., Stein, A., Stunder, B., 2017. Real-time environmental applications and display system Ready. Environmental Modelling Software 95, 210–228.
Roney, J.A., White, B.R., 2006. Estimating fugitive dust emission rates using an environmental boundary layer wind tunnel. Atmos. Environ. 40, 7668–7685.
Ryan, E., 2015. The public trust doctrine, private water allocation, and mono lake: the historic saga of national audubon society v. Superior Court. Environ. Law 45, 561.
Schaufler, G., Kitzler, B., Schindlbacher, A., Skiba, U., Sutton, M., Zechmeister-Boltenstern, S., 2010. Greenhouse gas emissions from European soils under different land use: effects of soil moisture and temperature. Eur. J. Soil Sci. 61, 683–696.
Service USDoASC, 1999. Soil taxonomy: a basic system of soil classification for making and interpreting soil surveys: US Department of Agriculture.
Shadkam, S., Ludwig, F., van Oel, P., Kirmit, Ç., Kabat, P., 2016. Impacts of climate change and water resources development on the declining inflow into Iran's Urmia Lake. J. Great Lakes Res. 42, 942–952.
Shao, Y., 2001. A model for mineral dust emission. J. Geophys. Res. Atmos. 106, 20239–20254.
Shao, Y., 2004. Simplification of a dust emission scheme and comparison with data. J. Geophys. Res. Atmos., 109
Shao, Y., Jung, E., Leslie, L.M., 2002. Numerical prediction of northeast Asian dust storms using an integrated wind erosion modeling system. J. Geophys. Res. Atmos., 107
Shao, Y., Lu, H., 2000. A simple expression for wind erosion threshold friction velocity. J. Geophys. Res. Atmos. 105, 22437–22443.
Shokri-Kuehni, S.M., Rad, M.N., Webb, C., Shokri, N., 2017a. Impact of type of salt and ambient conditions on saline water evaporation from porous media. Adv. Water Resour. 105, 154–161.
Shokri-Kuehni, S.M., Vetter, T., Webb, C., Shokri, N., 2017b. New insights into saline water evaporation from porous media: Complex interaction between evaporation rates, precipitation, and surface temperature. Geophys. Res. Lett. 44, 5504–5510.
Smith, P., 2008. Land use change and soil organic carbon dynamics. Nutr. Cycl. Agroecosyst. 81, 169–178.
Sørensen, M., 2004. On the rate of aeolian sand transport. Geomorphology 59, 53–62.
Steduto, P., Hsiao, T.C., Raes, D., Fereres, E., 2009. AquaCrop—The FAO crop model to simulate yield response to water: I Concepts and underlying principles. Agronomy J. 101, 426–437.
Thiessen, A.H., 1911. Precipitation for large areas. Mon. Weather Rev. 39, 1082–1084.
White, B.R., 1979. Soil transport by winds on Mars. J. Geophys. Res. Solid Earth 84, 4643–4651.
Williams, W.D., 1996. What future for saline lakes? Environ. Sci. Policy Sustain. Dev. 38, 12–39.

Williams, W.D., 2002. Environmental threats to salt lakes and the likely status of inland saline ecosystems in 2025. Environ. Conserv. 29, 154–167.
Winter, T.C., Buso, D.C., Rosenberry, D.O., Likens, G.E., Sturrock, A.J.M., Mau, D.P., 2003. Evaporation determined by the energy-budget method for Mirror Lake New Hampshire. Limnol. Oceanogr. 48, 995–1009.
WRMC, 2007. Master Plan Report on Agricultural Water in the Lake Urmia Basin (In Farsi). Water and Wastewater Planning Office, Iran.
Wurtsbaugh, W.A., Miller, C., Null, S.E., DeRose, R.J., Wilcock, P., Hahnenberger, M., et al., 2017. Decline of the world's saline lakes. Nat. Geosci. 10, 816.
Zilberman, T., Gavrieli, I., Yechieli, Y., Gertman, I., Katz, A., 2017. Constraints on evaporation and dilution of terminal, hypersaline lakes under negative water balance: The Dead Sea Israel. Geochim. Cosmochim. Acta 217, 384–398.